DOE F 241.3
(2-01) p.1 of 2

UNITED STATES DEPARTMENT OF ENERGY (DOE)
Announcement of Scientific and Technical Information (STI)
(For Use By Financial Assistance Recipients and Non-M&O/M&I Contractors)

OMB CONTROL NO. 1910-1400

PART I: STI PRODUCT DESCRIPTION
(To be completed by Recipient/Contractor)

A. STI Product Identifiers

1. REPORT/PRODUCT NUMBER(s)
None

2. DOE AWARD/CONTRACT NUMBER(s)
DE-FC36-97ID13554

3. OTHER IDENTIFYING NUMBER(s)
None

B. Recipient/Contractor

Steel Research Centre, McMaster University,1280 Main St. West, Hamilton, Ontario, Canada L8S 4L7

C. STI Product Title

Nitrogen Control in Electric Arc Furnace Steelmaking by DRI Fines Injection

D. Author(s)

Irons, Dr. Gordon A.

E-mail Address(es):
ironsga@mcmaster.ca

E. STI Product Issue Date/Date of Publication

03 31 2004
MM DD YYYY

F. STI Product Type (*Select only one*)

☒ 1. TECHNICAL REPORT
☒ *Final* ☐ *Other (specify)* _____

☐ 2. CONFERENCE PAPER/PROCEEDINGS

Conference Information (title, location, dates)

☐ 3. JOURNAL ARTICLE
a. TYPE: ☐ *Announcement Citation Only* ☐ *Preprint* ☐ *Postprint*
b. JOURNAL NAME
c. VOLUME _____ *d. ISSUE* _____
e. SERIAL IDENTIFIER (e.g. ISSN or CODEN)

☐ 4. OTHER, SPECIFY

G. STI Product Reporting Period

11 01 2001 Thru 03 31 2004
MM DD YYYY MM DD YYYY

H. Sponsoring DOE Program Office

Office of Industrial Technologies (OIT)(EE20)

I. Subject Categories *(list primary one first)*

32 Energy Conservation, Consumption and Utilization

Keywords: Steel, Electric Arc Furnace (EAF), Nitrogen, Direct Reduced Iron (DRI)

J. Description/Abstract

A novel way to make low nitrogen content steel in electric arc furnaces was investigated involving the injection of direct reduced iron fines into steel to produce fine bubbles that absorbed nitrogen. Recommendations on the best DRI size, composition, amount and injection conditions are made.

K. Intellectual Property/Distribution Limitations

(must select at least one; if uncertain contact your Contracting Officer (CO))

☒ 1. UNLIMITED ANNOUNCEMENT *(available to U.S. and non-U.S. public; the Government assumes no liability for disclosure of such data)*

☐ 2. COPYRIGHTED MATERIAL: *Are there any restrictions based on copyright?* ☐ *Yes* ☐ *No.*
If yes, list the restrictions as contained in your award document

☐ 3. PATENTABLE MATERIAL: THERE IS PATENTABLE MATERIAL IN THE DOCUMENT.
INENTION DISCLOSURE SUBMITTED TO DOE:
DOE Docket Number: S-
(Sections are marked as restricted distribution pursuant to 35 USC 205)

☐ 4. PROTECTED DATA: ☐ CRADA ☐ *Other, specify*
Release date (required) no more than 5 years from date listed in Part I.E. above ___ ___ ____ (MM DD YYYY)

☐ 5. SMALL BUSINESS INNOVATION RESEARCH (SBIR) DATA
Release date (required) no more than 4 years from date listed in Part I.E. above ___ ___ ____ (MM DD YYYY)

☐ 6. SMALL BUSINESS TECHNOLOGY TRANSFER RESEARCH (STTR) DATA
Release date (required) no more than 4 years from date listed in Part I.E. above ___ ___ ____ (MM DD YYYY)

☐ 7. OFFICE OF NUCLEAR ENERGY APPLICED TECHNOLOGY

L. Recipient/Contract Point of Contact *Contact for additional information (contact or organization name To be included in published citations and who would Receive any external questions about the content of the STI Product or the research contained herein)*

Dr. Gordon Irons – Principal Investigator,
Name and/or Position
ironsga@mcmaster.ca *(905) 525-9140 x24974*
E-mail *Phone*
Steel Research Centre, McMaster University, Hamilton, ON, Canada L8S 4L7

UNITED STATES DEPARTMENT OF ENERGY (DOE)
Announcement of Scientific and Technical Information (STI)
(For Use By Financial Assistance Recipients and Non-M&O/M&I Contractors)

OMB CONTROL NO.
1910-1400

PART II: STI PRODUCT MEDIA/FORMAT and LOCATION/TRANSMISSION

(To be completed by Recipient/Contractor)

A. Media/Format Information:

1. MEDIUM OF STI PRODUCT IS:
   ☒ Electronic Document ☐ Computer Medium
   ☐ Audiovisual Material ☒ Paper ☐ No Full-text
2. SIZE OF STI PRODUCT 54 Pages
3. SPECIFY FILE FORMAT OF ELECTRONIC DOCUMENT BEING TRANSMITTED, INDICATE:
   ☐ SGML ☐ HTML ☐ XML ☒ PDF Normal
   ☐ PDF Image ☐ TIFFG4
   ☐ WP-indicate Version (*5.0 or greater)* _____
   Platform/operation system _____
   ☐ MS-indicate Version (*5.0 or greater)* _____
   Platform/operation system _____
   ☐ Postscript _____
4. IF COMPUTER MEDIUM OR AUDIOVISUAL MATERIAL:
   a. Quantity/type (*specify)* _____
   b. Machine compatibility (*specify)* _____
   c. Other information about product format a user needs to know:
   _____

B. Transmission Information:

1. STI PRODUCT IS BEING TRANSMITTED:
   ☐ a. Electronically via E-Link
   ☒ b. Via mail or shipment to address indicated in award document (*Paper product, CD-ROM, diskettes, video cassettes, etc.)*
   _____
2. INFORMATION PRODUCT FILE NAME
   ☒ *(of transmitted electronic format)*
   EditedTRP9807FinalReport.

PART III: STI PRODUCT REVIEW/RELEASE INFORMATION

(To be completed by DOE)

A. STI Product Reporting Requirements Review.

☐ 1. THIS DELIVERABLE COMPLETES ALL REQUIRED DELIVERABLES FOR THIS AWARD
☐ 2. THIS DELIVERABLE FULFILLS A TECHNICAL INFORMATION REPORTING REQUIREMENT, BUT SHOULD NOT BE DISSEMINATED BEYOND DOE.

B. Award Office Is the Source of STI Product Availability

☐ THE STI PRODUCT IS NOT AVAILABLE IN AN ELECTRONIC MEDIUM. THE AWARDING OFFICE WILL SERVE AS THE INTERIM SOURCE OF AVAILABILITY.

C. DOE Releasing Official

☐ 1. I VERIFY THAT ALL NECESSARY REVIEWS HAVE BEEN COMPLETED AS DESCRIBED IN DOE G 241.1-1A, PART II, SECTION 3.0 AND THAT THE STI PRODUCT SHOULD BE RELEASED IN ACCORDANCE WITH THE INTELLECTUAL PROPERTY/DISTRIBUTION LIMITATION ABOVE.

Release by (*name)* _____

Date ___ ___ _____
MM DD YYYY

E-Mail _____

Phone _____

AISI/DOE Technology Roadmap Program

Final Report

Nitrogen Control in EAF Steelmaking by DRI Fines Injection

By

Dr. Gordon A. Irons & Dorel Anghelina – McMaster University
Dr. Geoffrey A. Brooks – CSIRO Minerals

March 31, 2004

Work Performed under Cooperative Agreement
No. DE-FC36-97ID13554
Prepared for
U.S. Department of Energy

Prepared by
American Iron and Steel Institute
Technology Roadmap Program Office
Pittsburgh, PA 15220

DISCLAIMER

Number of pages in this report: 54

DOE and DOE contractors can obtain copies of this report FROM: Office of Scientific and Technical Information, P. O. Box 62, Oak Ridge, TN 37831. (615) 576-8401.

This report is publicly available from the Department of Commerce, National Technical Information Service, 5285 Port Roya l Road, Springfield, VA 22161. (703) 487-4650.

Nitrogen Control in EAF Steelmaking by DRI Fines Injection

by:

Dorel Anghelina, Geoffrey A. Brooks* & Gordon A. Irons
Steel Research Centre
McMaster University
Hamilton, Ontario
Canada, L8S 4L7

*currently with
CSIRO Minerals
Clayton, Victoria
Australia

A Final Report

Prepared for

American Iron & Steel Institute and
Department of Energy
Technology Roadmap Program
Project # 0009
Cooperative Agreement DE-FC36-97ID13554

March 31, 2004

Title: Nitrogen Control in EAF Steelmaking by DRI Fines Injection

Authors: Dorel Anghelina, Geoffrey A. Brooks and Gordon A. Irons

Performing Organization Names, Addresses:

Steel Research Centre
McMaster University
1280 Main Street West
Hamilton, ON
L8S 4L7

Abstract:

Nitrogen is difficult to remove in electric arc furnace (EAF) steelmaking, requiring the use of more energy in the oxygen steelmaking route to produce low-nitrogen steel. The objective of this work was to determine if the injection of directly reduced iron (DRI) fines into EAFs could reduce the nitrogen content by creating fine carbon monoxide bubbles that rinse nitrogen from the steel. The proposed work included physical and chemical characterization of DRI fines, pilot-scale injection into steel, and mathematical modeling to aid in scale-up of the process. Unfortunately, the pilot-scale injections were unsuccessful, but some full-scale data was obtained. Therefore, the original objectives were met, and presented in the form of recommendations to EAF steelmakers regarding:

- **The best composition and size of DRI fines to use;**
- **The amount of DRI fines required to achieve a specific reduction in nitrogen content in the steel; and**
- **The injection conditions.**

This information may be used by steelmakers in techno-economic assessments of the cost of reducing nitrogen with this technology.

(RDP Standard Form, Form 298)

EXECUTIVE SUMMARY

This study was undertaken to determine if the injection of (Directly Reduced Iron) DRI fines could be an effective way to remove nitrogen from electric furnace steel. The proposed work consisted of three aspects:

- Materials characterization to determine the best composition for the DRI fines;
- Injection trials in a 60-kg induction furnace to determine the effects of injection variables on nitrogen removal; and
- Mathematical modeling to quantify the results and aid in scale-up.

The Materials Characterization work (Chapter 2) showed that the carbon and oxygen contents of the DRI fines should be stoichiometrically balanced to generate CO, and furthermore these contents should be maximized. The detrimental effects of gangue content of the DRI were identified.

A Thermodynamic analysis (Chapter 3) identified the quantity of DRI required for various extents of removal of nitrogen.

Unfortunately, it proved impossible to inject the DRI fines into the induction furnace, despite numerous trials, and it was decided mutually by the investigators and sponsors to terminate this phase of the work (Chapter 4).

A Kinetic Model was developed in Chapter 5 that showed that the removal of nitrogen from steel into CO bubbles is very rapid, and the bubbles become saturated in a very short rise. Consequently, the equilibrium or thermodynamic analysis in Chapter 3 can be used without the use of a complex kinetic model. Analysis of industrial data (previous North Star Steel data, and new data supplied by Hamburger Stahlwerke) supported these findings.

In Chapter 6, a fluid mechanic model for the penetration of a gas-particle jet was adapted to this system to aid in the selection of the injection conditions (lance diameter, solids flow rate, gas-to-solids ratio, and lance angle). The results are presented graphically to select the injection conditions.

In Chapter 7, recommendations are made for:

- The best composition and size of DRI fines to be used;
- The amount of DRI fines required to achieve a specific reduction in nitrogen content in the steel; and
- The injection conditions.

There is enough information in this report for individual steel companies to make their own techno-economic assessments of the cost of reducing nitrogen with DRI fines injection. These assessments are very site specific regarding the local cost and quality of DRI fines, the economic benefit of reduced nitrogen for the steel products made (or that could be made with

lower nitrogen capability), and the availability and cost of the injector and associated lance equipment.

Finally, the Conclusions of the work are summarized in Chapter 8.

LIST OF FIGURES

LIST OF TABLES

TABLE OF CONTENTS

1. INTRODUCTION

Nitrogen even in small quantities is detrimental to the quality of steel. Traditionally, the blast furnace (BF)/basic oxygen furnace (BOF) steelmaking route has been favored over the electric arc furnace steelmaking (EAF) route for the production of high-quality steels, partially due to the lower nitrogen level. Steel produced from a BOF contains 30 to 40 ppm, N compared to 70 to 100 ppm N in an EAF.

Increasingly, there is a need to produce quality steels via EAFs because of the lower energy and operating costs. This project aims to overcome the hurdle for the production of low-nitrogen steel in an EAF.

The goal of this work was to develop a technique for nitrogen removal from liquid steel by injection of DRI fines. DRI fines, generated either directly from DRI process or by attrition in transport or handling, contain significant quantities of carbon and oxygen. Studies have shown that upon heating these elements react rapidly inside DRI particles to form fine CO bubbles. Fine CO bubbles are very effective in removing nitrogen dissolved in steel. This potential benefit is largely lost when DRI enters a steel bath in the form of pellets and briquettes. The evolved CO at the top surface has insufficient contact with the melt to allow significant removal of dissolved nitrogen.

The main sources of dissolved nitrogen into molten steel are:

- presence of nitrogen in the feed materials (notably steel scrap);
- exposure of molten steel to air, and
- exposure of molten steel to ionized nitrogen in a plasma.

The judicious blending of feed materials alleviates partially the nitrogen problem, as direct reduced iron (DRI) contains significantly less nitrogen than scrap. Nitrogen pick-up by exposure to the atmosphere can also be minimized by operational conditions (foamy slag and tapping practice). High-powered furnaces with long arcs are particularly susceptible to pick-up, namely due to the nitrogen dissociation in the arc, promoting nitrogen absorption into the bath [1].

The main options for removing the accumulated nitrogen during EAF processing are as follows:

- vacuum degassing in a subsequent ladle operation;
- addition of nitride forming elements in a ladle operation, and
- rinsing with bubbles of CO or other gases in the molten steel.

Vacuum degassing is currently the dominant technology for removing nitrogen although it has disadvantages: time consuming (thus compromising productivity) and expensive removal with limited efficiency [2].

The addition of nitriding elements to form inclusions has proven disappointing in industrial trials, as the concentration of inclusions is so low that agglomeration in inclusions is limited. Consequently, the rate of flotation of the inclusions limits removal of nitrogen [2].

It is well established that CO bubbles passing through a steel melt have a scrubbing effect on dissolved nitrogen, as nitrogen is readily absorbed into CO bubbles. Carbon monoxide can be generated in many ways. The main method is the addition of iron-carbon compounds contained in commercial products, such as DRI and iron carbide. These compounds also contain unreduced iron oxides that serve as a source of oxygen for the formation of fine CO bubbles by an "internal" decarburization reaction, namely:

$$O_{(DRI-gangue)} + C_{(DRI-Fe)} \rightarrow CO_{(g)} \qquad (1)$$

Thermogravimetric studies of DRI fines and iron carbide have shown that "internal decarburization" commences above 800 °C, possibly due to physical changes inside the DRI particles [3 - 4].

Goldstein *et al*. studied the addition of DRI pellets to remove nitrogen from steel, and quantified the fundamental kinetics of nitrogen removal by CO bubbling [5]. They concluded that nitrogen removal effects of CO bubbling from the decarburization reaction in DRI were largely lost in steelmaking operations because the bubbles are generated high in the melt as a result of the buoyancy of DRI pellets. These results further emphasize the potential advantages of injecting DRI fines deep into steel melt, as opposed to continuous feeding or batch charging of DRI pellets.

The present study examines the generation of CO by the injection of DRI fines; these fines are generated inevitably from the handling and transportation of DRI pellets and briquettes, but such fines could be specifically prepared by crushing DRI pellets. It should be noted that some EAF shops already inject DRI fines to gain some value from this degraded product [6]. To our knowledge there have been no studies to isolate the effect of fines injection, and to optimize this process for nitrogen removal.

Iron carbide has been injected in a number of trials by North Star Steel and Nucor; there have been reported significant removal of nitrogen, from 80 ppm to 30 ppm, without adversely affecting metal quality or reducing overall energy usage [7 - 11]. As the iron carbide cannot be economically produced, the industry is looking for replacement for iron carbide for nitrogen removal. Iron carbide is thought to remove nitrogen by the rinsing action of fine CO bubbles generated by deep injection of iron carbide; this work seeks to generate the same effect with DRI fines.

Previous research on powder injection processes for hot metal desulfurization has shown that typically only 30 to 50 % of the injected powders actually contact the metal to accomplish reaction such as desulfurization [12]. The contact is improved to 100% when there is significant gas evolution, that pushes the particles into contact with the melt, and thereby further increasing turbulence and contact. Therefore, the injection of DRI fines with excess

carbon and oxygen to create carbon monoxide should be an excellent candidate for the creation of gas deep in the melt. In contrast to pellet feeding, [13 – 14], the DRI fines injection the heating rate will be virtually instantaneous, and it is expected that the CO evolution rate will be limited only by the injection rate.

In the original proposal there were two parallel streams. The first stream was to fully characterize DRI fines available from industrial sources using sieving, microscopy, and XRD, XRF and thermogravimetric analysis. Of particular importance was the overall chemistry (including nitrogen and sulfur contents), size characteristics and behavior during rapid heating.

The second stream was to be the injection of DRI fines into steel to investigate the effects of:

- particle size distribution;
- solid and gas injection rates;
- lance depth;
- sulphur content of steel;
- temperature; and
- initial nitrogen content of steel.

It was proposed to develop a predictive mathematical model for nitrogen removal based on the injection parameters and chemical considerations, and plant trials were to be explored with the participating AISI members in a follow-up program.

2. MATERIALS CHARACTERIZATION

2. 1. Composition and stoichiometry

Since the objective of this work is to generate CO from the DRI fines, the carbon and oxygen contents are of prime importance; they are plotted against one another in Figure 1. The "Stoichiometric Line" provides the composition boundary based on pure Fe_3O_4, since Fe_2O_3 is so easily reduced, and pure Fe_3C, assuming no free carbon is present. The CO_2 and CO lines represent compositions balanced to produce these gases from the material; conditions in steelmaking are so reducing that virtually pure CO is produced. Therefore, materials below the CO line have excess carbon, and those above excess oxygen. The compositions of two types of iron carbide [3 - 4, 15 - 16], and the two bulk DRI materials used in this study are superimposed on Figure 1. The lines parallel to the Stoichiometric line show the relative amount of gas released to this maximum (0.0943 $Nm^3\ kg^{-1}$). Clearly, the iron carbide materials release more CO than the DRI materials, but the iron carbide materials cannot be made commercially. The Midrex DRI is well balanced for CO production, whereas the Ispat material is oxygen deficient.

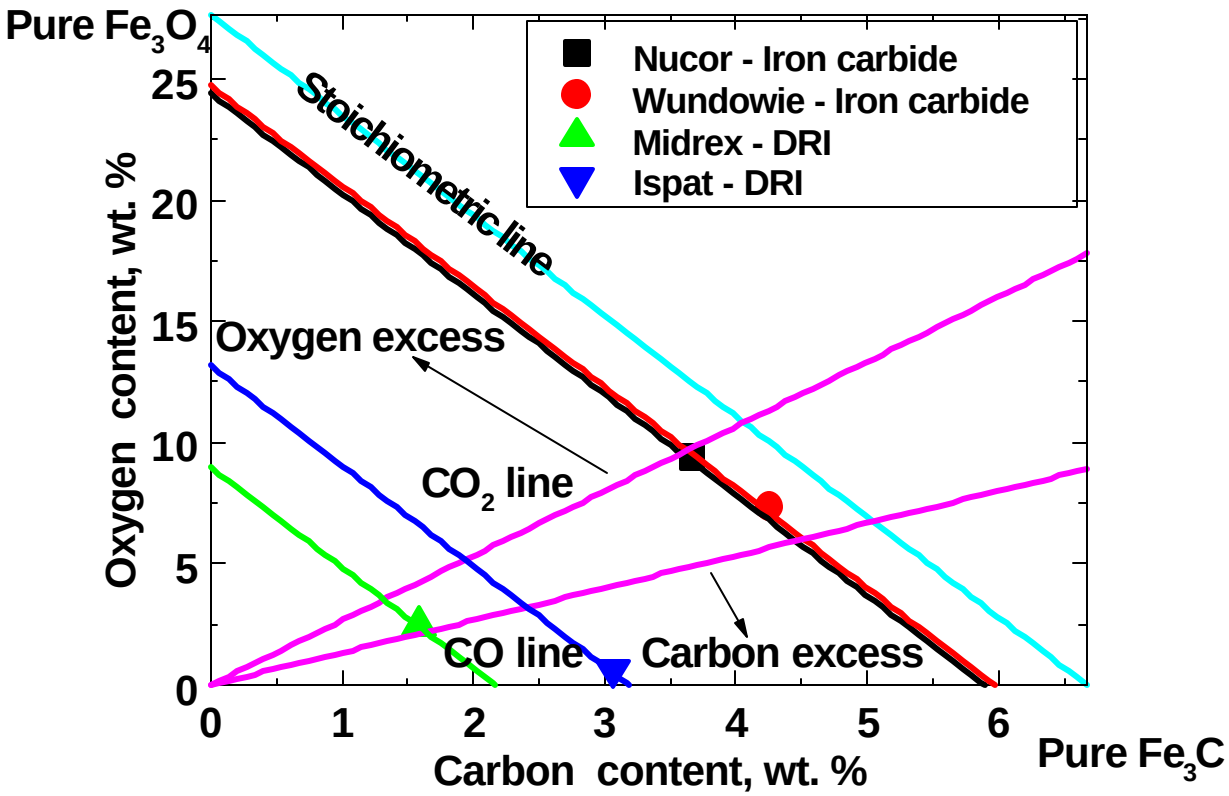

Figure 1. Range of compositions for iron carbide and DRI products.

The gas generation is better described in Table I. The second column shows the sum of the carbon and oxygen contents. The weight loss observed by thermogravimetric analysis is always less than this amount (column 3). The stoichiometric weight loss will be controlled by the minimum of either the carbon or oxygen which is expressed mathematically as:

$$W_L = \min\left(C, \frac{12}{16} \times O\right) + \min\left(C \times \frac{16}{12}, O\right) \qquad \left[wt.\ \%\right] \qquad (2)$$

This information is contained in column 4, and it can be converted to the gas release by:

$$R_G = \frac{W_L}{100} \times \left(\frac{22.4}{28}\right) \text{ Nm}^3 \text{ kg}^{-1} \text{ DRI.}$$

Table I. Comparison of weight loss and gas generation for various materials (The weight loss by thermogravimetric analysis at heating rates of 5 °C min^{-1} (*) and 50 °C min^{-1} (**))

Material	**C + O (tot) wt. %**	**Weight Loss (%)**	**C + O (stoich.) wt. %**	R_G (100 % CO) **Nm^3 kg^{-1}**
Nucor	13.0	7.6	8.55	0.0684
Wundowie	11.6	N/A	9.93	0.0794
Midrex*	< 4.5	3.27	3.69	0.0295
Midrex**	< 4.5	3.85	3.69	0.0295
Ispat 1**	< 5.0	3.10	2.95	0.0236
Ispat 2**	6.66	5.34	6.53	0.0522

The stoichiometric weight loss is still less than that observed due to kinetic factors that will be addressed in the next section.

2. 2. <u>High temperature behavior of DRI fines</u>

2. 2. 1. Experimental procedure

Two different DRI fines sources were obtained from commercial sources; they shall be referred to as Midrex Bulk (MB) and Ispat Bulk (IB). The Midrex sample was split into two size fractions, Midrex Fine (MF) and Midrex Coarse (MC). The following techniques were used to characterize these materials:

(i) Size analysis using standard sieving techniques.

(ii) Moisture was determined by weighing samples before and after heating to 200 °C.

(iii) Chemical analysis for iron using a standard titration technique. Dissolution in HCl was used to determine total iron content and separation with copper sulfate solution was used to determine the metallic iron content. The filtered residue from this operation was

treated by sulfuric acid and a value for Fe^{2+} was obtained from titration. The concentration of Fe^{3+} was calculated by subtracted the values obtained for metallic Fe and Fe^{2+} from the total Fe determination.

(iv) LECO analysis was used to determine the carbon, sulfur and nitrogen content of the samples. A LECO CS-444 analyzer was used for carbon and sulfur, and a LECO TC-136 analyzer was used for nitrogen. Standard procedures were followed in all cases using commercially supplied standards.

(v) Gangue content was determined by dissolving 2 g samples into HCl, separating the residue by filtering and heating this material in a platinum crucible to 940 °C to remove carbon. This material was dissolved in HF acid to remove silica and this residue fired to determine the total gangue.

(vi) Powder X-ray Diffraction (XRD) performed in a X-Rays Nicolet Diffractometer with CuKα radiation and standard slit geometry was used to identify the major crystalline phases present in the materials.

(vii) Simultaneous thermogravimetric (TG) and differential thermal analysis (DTA) was performed on a Netzsch STA 409 PC. Samples were flushed with Ar whilst being heated from 20 to 1400 °C. Two heating rates were used, 5 °C min^{-1} and 50 °C min^{-1}. An alumina sample was used as the reference sample.

2. 2. 2. Experimental results

The significant results obtained from chemical and thermogravimetric results for the four samples, Midrex Fine, Midrex Coarse, Midrex Bulk and Ispat Bulk, are summarized in Table II. The TG-DTA curves obtained for three of the samples are shown in Figures 1, 2 and 3. Table III and Table IV summarizes the key features of these curves. Table V presents the results of the chemical analysis of Fe^{2+} and Fe^{3+} in the various samples.

These results show that Midrex Coarse has marginally higher total iron than the Midrex Bulk and Midrex Fines, though all the Midrex fraction have higher iron content than Ispat Bulk. The total metallic content is relatively consistent between all four samples, meaning that the Midrex sample must contain more non-metallic iron in the form of magnetite and hematite. This observation is consistent with the lower available oxygen calculated from the titration carried out to determine Fe^{2+} and Fe^{3+} concentrations. The concentrations of the ferrous and ferric ions in the DRI samples, summarized in Table V, show that the Midrex material is more highly oxidized than the Ispat material. This means that the carbon in the Ispat Bulk material should become starved of oxygen during heating, at least until temperatures above 1400 °C when some of the other gangue materials may undergo reduction. XRD of the samples showed that α Fe was the dominant phases present in all samples, though both magnetite and hematite were detectable in the Midrex samples.

Table II. Summary of Characterization of DRI fines.

Parameter/Material	Midrex Fine	Midrex Coarse	Midrex Bulk	Ispat Bulk
d_p, m $\times 10^{-6}$	38 – 45	2360 – 3350	38 -3350 (1430*)	38 – 3350 39 (72*)
Fe_{tot}, wt. %	94.5 ± 1.1	95.2 ± 1.1	93.6 ± 1.1	89.6 ± 0.93
Fe_{met}, wt. %	87.2	88.6	87.5	87.7
C, wt. %	1.99	1.33	1.59	3.06
O**, wt. %	2.92	2.61	2.43	0.64
S, wt. %	Max. 0.03	Max. 0.03	Max. 0.03	Max. 0.0125
N, ppm	N/A	N/A	N/A	30.0
Gangue, wt. %	2.9	3.3	4.0	2.7
SiO_2, wt. %	0.8	0.7	0.6	1.3
Moisture, wt. %	0.37 ± 0.1	0.44 ± 0.1	0.45 ± 0.1	0.34 ± 0.07

Note: *- average particle size; ** - calculated from Fe^{2+}/Fe^{3+} mix using the titration method.

The thermogravimetric analysis revealed three distinct regions of mass loss during heating of the fines. As can be seen clearly in Figures 1, 2 and 3, there are three distinct region of the curves for the three samples studied. In region I, commencing between 180 °C and 250 °C, a small weight loss was shown in all samples. This weight loss corresponded to less than 0.25 wt. % of the total weight and less than 7% of the total weight loss. It is interesting to note that the smallest weight change (3% of total weight loss) associated with this region was found for the Ispat Bulk sample, which had the lowest iron oxide content of the samples. This observation suggests that the larger weight loss for Midrex samples in region I is associated with some reduction of hematite to magnetite under the reducing conditions of the TG analysis.

Region II, commencing between 510 °C and 580 °C, represented the start of significant reduction in weight, with rapid acceleration of the reaction rate until slowing and than commencing of region III between 770 °C and 860 °C. After the acceleration of region III, the weight loss curves flattened out until the final temperature of 1400 °C. In all cases the total weight loss associated with the third region was greater in region III compared to region II, as can been seen Table IV.

Table III. Data for onset temperatures of mass loss from TG-DTA analysis of DRI.

Sample	Region I °C	Region II °C	Region III °C
Midrex Bulk*	249	514	774
MidrexBulk**	235	575	855
Ispat Bulk**	183	542	837

Note: * - 5 °C min^{-1}, ** - 50 °C min^{-1}.

Table IV. Mass loss data for TG-DTA analysis of DRI fines.

Sample	Region I abs %	Region II abs %	Region III abs %	Moisture wt. %	Total wt. %
Midrex Bulk*	0.11	1.16	1.69	0.45	3.27
Midrex Bulk**	0.23	1.02	2.05	0.45	3.85
Ispat Bulk**	0.08	0.59	2.10	0.34	3.10

Note: * - 5 °C min^{-1}, ** - 50 °C min^{-1}.

Table V. Ferrous and ferric ions in various DRI materials (wt.%).

Material type	Fe^{2+}	Fe^{3+}
Midrex Bulk	1.61	4.58
Midrex Coarse	1.57	5.02
Midrex Fine	1.26	5.96
Ispat 1 Bulk	1.06	0.79

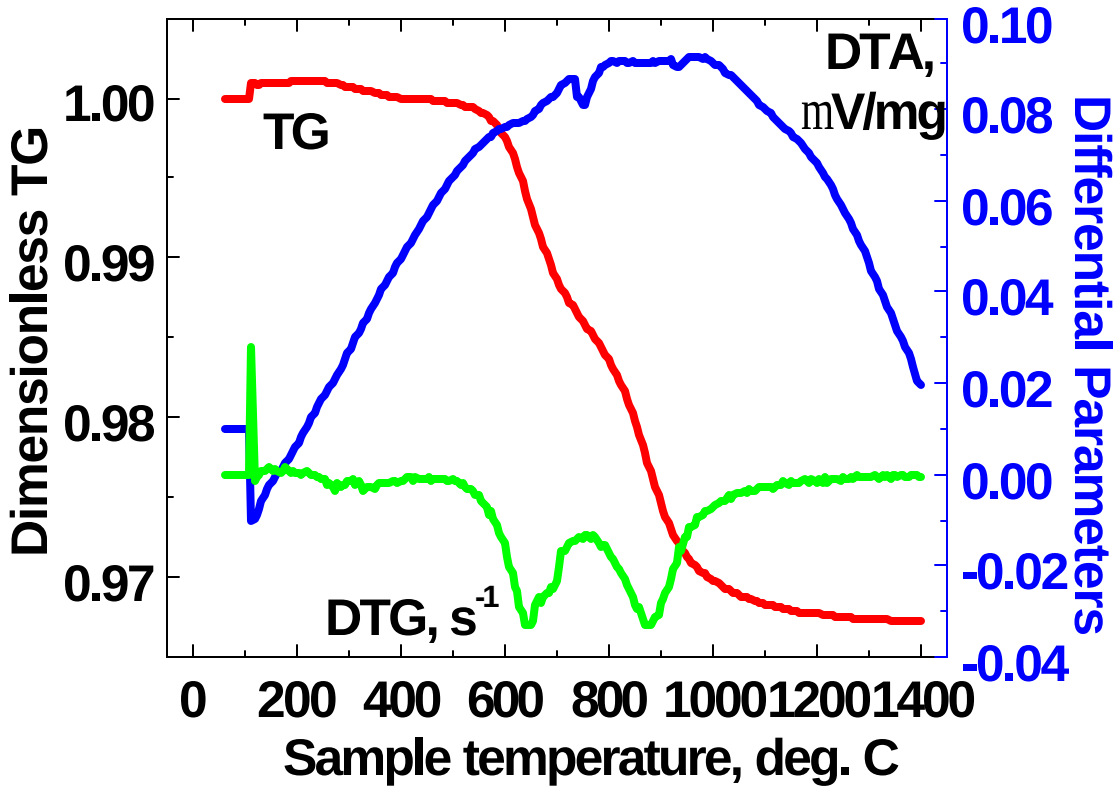

Figure 2. TG-DTA curve for Midrex Bulk at 5 °C min^{-1}.

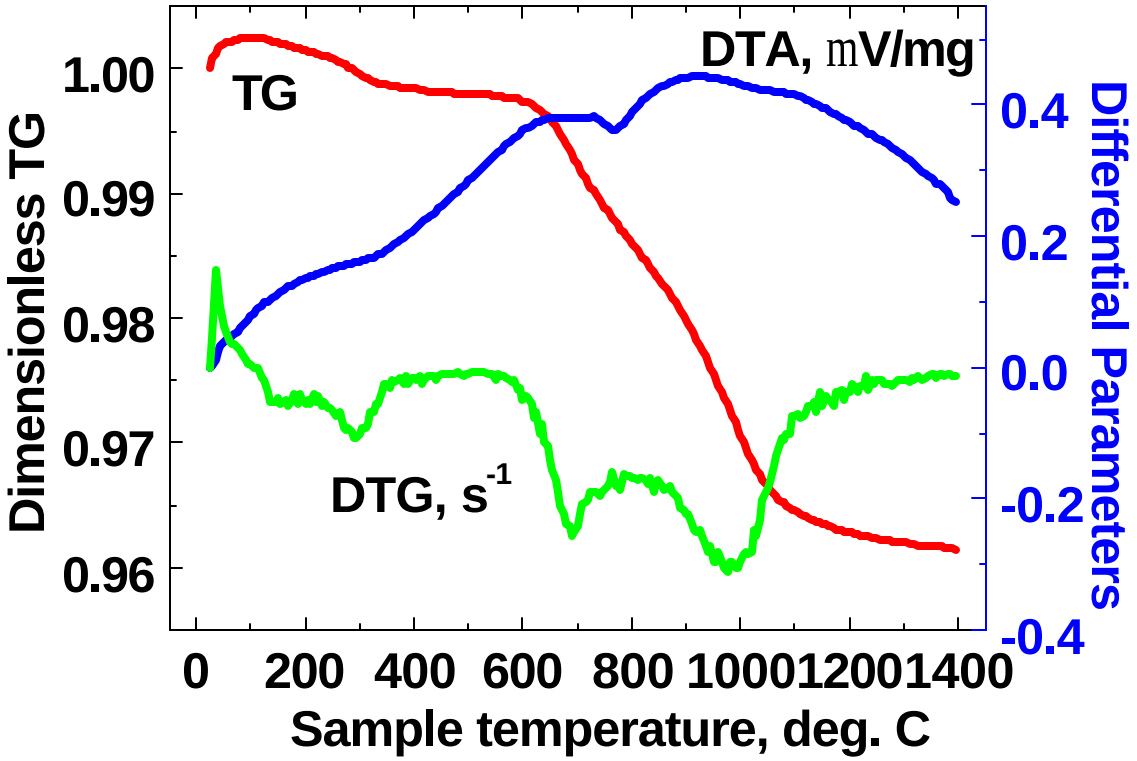

Figure 3. TG-DTA curve for Midrex Bulk at 50 °C min^{-1}.

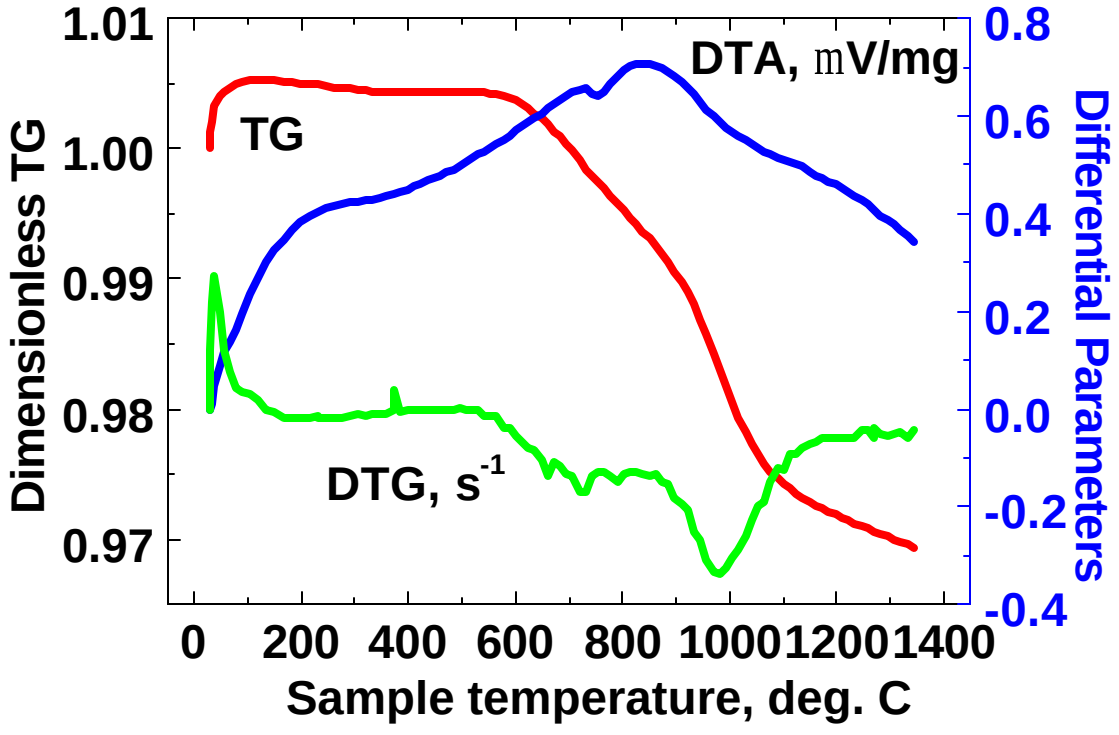

Figure 4. TG-DTA curve for Ispat Bulk at 50 °C min^{-1}.

2. 3. Thermodynamic Modelling

Thermodynamic modeling of the system was carried out using FACT Version 2.1 software. FACT is a well established integrated modeling package based on a Gibbs Energy minimization routine with a large thermodynamic database that include activity data for both solids and liquids.

In this "virtual experiment", starting compositions of materials were "heated" in increments of 50 °C, and at each step a new equilibrium composition is determined, and the evolved gases were allowed to escape.

The following assumptions were used:

i) the system was isothermal and reached equilibrium at each step,
ii) the gas phase was removed from the solid phases between each equilibrium calculation,
iii) moisture was neglected,
iv) 0.5 g of DRI material was used,
v) 0.005 moles (120 cm^3) of Ar atmosphere at 1 atm pressure was the initial atmosphere, and
vi) liquid phases were disregarded.

Two starting compositions were considered; they are summarized in Table VI.

The results of the modeling are summarized in Figures 4 and Figures 5.

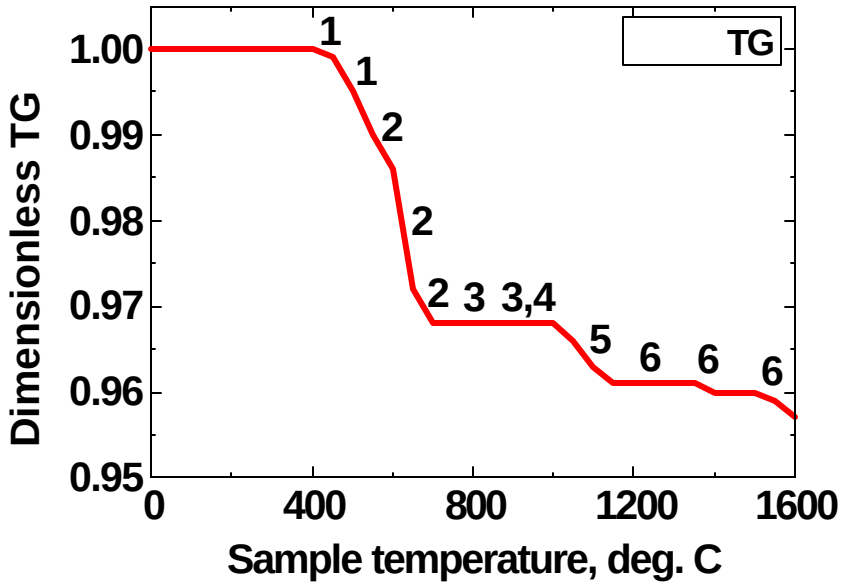

Figure 5. Predicted thermogravimetric curve for 2 wt. % oxygen as iron oxides (numbers indicate the associated reactions from Table VII).

Table VI. Starting DRI Compositions for Thermodynamic Modeling.

Element/Material type	2 wt. % oxygen	3 wt. % oxygen
C	1.59	1.59
Fe_2O_3	6.7	10.0
SiO_2	2.5	2.5
O	2.0	3.0
Fe	89.3	85.9

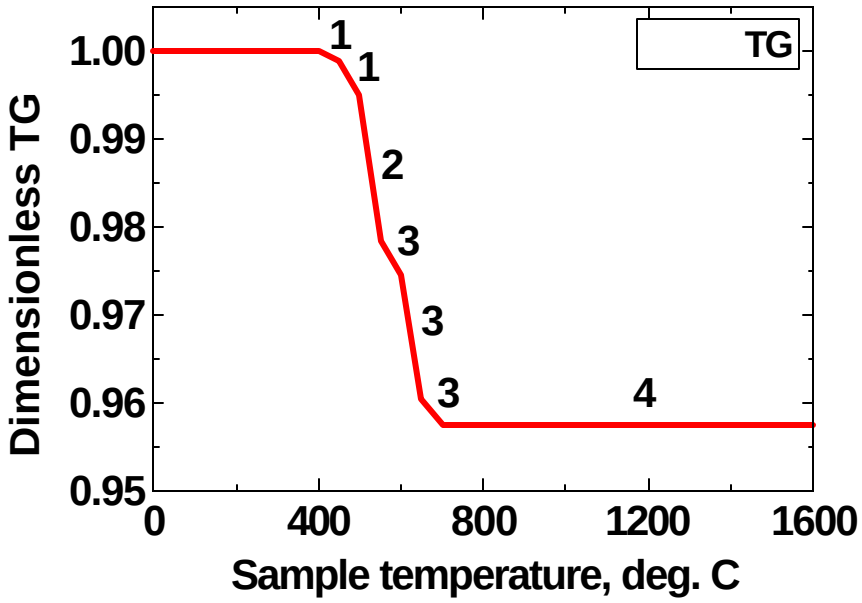

Figure 6. Predicted thermogravimetric curve for 3 wt. % oxygen as iron oxides (numbers indicate the associated reactions from Table VIII).

Table VII. DRI reactions during sample heating (2 wt. % oxygen as iron oxides – Figure 5).

#	Temperature range, °C	Reaction
1.	350 – 550	$Fe_3O_4 + 4\ C \rightarrow 3\ Fe + 4\ CO$ (Fe_3O_4 is consumed)
2.	550 – 650	$(2\ FeO) \bullet SiO_2 + 2\ C \rightarrow 2\ Fe + SiO_2 + 2\ CO$ ($(2\ FeO) \bullet SiO_2$ consumed; carbon still exists)
3.	650 – 900	No reduction for iron oxide(s)
4.	750 – 900	$SiO_2 + Fe + 2\ C \rightarrow FeSi + 2\ CO$
5.	900 – 1100	$2\ Fe_3C + SiO_2 \rightarrow FeSi + 5\ Fe + 2\ CO$ (carbon is consumed)
6.	1100 – 1600	$FeSi + SiO_2 \rightarrow Fe + 2\ SiO$ (SiO vaporization)

Table VIII. DRI reactions during sample heating (3 wt. % oxygen as iron oxides – Figure 6) (* - fractions for FeO and Fe are also variables for the temperature range).

#	**Temperature range, °C**	**Reaction**
1.	350 – 550	$Fe_3O_4 + 4\ C \rightarrow 3\ Fe + 4\ CO$
2.	≅ 550	$Fe_3O_4 + x\ C \rightarrow (4 - x)\ FeO + (x - 1)\ Fe + x\ CO$ *
3.	550 – 700	$(2\ FeO) \bullet SiO_2 + 2\ C \rightarrow 2\ Fe + SiO_2 + 2\ CO$ (carbon is consumed; end of iron oxides reduction; fayalite in excess)
4.	- 1600	Fe vaporization

These curves show predict rapid weight loss from reaction between carbon and iron oxides above 500 °C. In the case of 3 wt.% O, the reaction is completed by 700 °C. At the lower initial oxygen content, starvation of oxygen from reaction between FeO and C, results in a staged reduction in weight as reaction between iron carbide and silica allows CO to be formed.

In conclusion, the characterization and modeling of DRI fines has established the following:

- Rapid generation of CO from internal reduction reactions in DRI fines commences above 500 °C.
- With sufficient stoichiometric oxygen from iron oxides available for reaction with carbon, equilibrium calculations predict that gas generation would be completed by 700 °C.
- The generation of gas was still observed well above 700 °C for all samples reflecting both kinetic restrictions for these reactions but also, in some cases, starvation of oxygen within the fines.
- The ratio of available oxygen to carbon is the most important characteristic of DRI fines in terms of the nitrogen removal capability of the material.

The work in this Chapter supports the initial premise that CO is generated from DRI fines, and the subsequent chapters examine the removal of nitrogen from steel by the CO.

3. THERMODYNAMIC ANALYSIS

3. 1. Nitrogen removal from steel with a carrier gas

There have been a number of studies that have examined nitrogen removal from steel with iron carbide and/or DRI [2 - 3, 8, 10, 16 - 18] with varying degrees of thermodynamic analysis. The purpose of this section is to summarize what is known about the thermodynamic limits to the removal of nitrogen with DRI, and make some calculations specific to conditions in the EAF.

In 1943 Geller [19] performed the earliest thermodynamic analysis of flushing nitrogen from steel, and there were a couple of additional studies prior to the recent interest in DRI [20 - 21].

The main reaction for the removal of dissolved nitrogen into gas bubbles is Sievert's law:

$$\underline{N} \leftrightarrow \tfrac{1}{2}\{N_2\} \qquad (3)$$

The equilibrium constant for reaction (3) is well established as described in *Appendix 1;* the accepted value is 22.22 $atm^{1/2}$ % N^{-1}. At one atmosphere of pure nitrogen pressure, 450 ppm $\underline{N}$ dissolves in pure iron at 1600°C.

Because the dissolved nitrogen partial pressure in a rising bubble is generally low, the spontaneous removal from the liquid steel is very limited. During bubble rise, the total pressure in the bubble decreases, at the same time as the nitrogen partial pressure in the bubble increases. Therefore, the partial pressure of nitrogen in the bubble needs to be considered. The bubble will contain other gases which we will call "carrier gas" which flush the nitrogen from the steel and push equation (3) to the right. In the present application, the carrier gas is the evolved CO from the DRI decomposition and the pneumatic conveying gas for the DRI particles. The nitrogen partial pressure is:

$$p_{N_2} = p_{tot} \times \left(\frac{vol.\ \%\ N_2}{100} \right) \qquad [atm] \qquad (4)$$

To convert the nitrogen partial pressure to the nitrogen removal rate, it is convenient to define a nitrogen gas flow rate, Q_{N_2} ($Nm^3\ s^{-1}$) and relate it to the carrier gas flow rate, Q_{CO} (considered to be only CO for simplicity):

$$p_{N_2} = \left(\frac{Q_{N_2}}{Q_{N_2} + Q_{CO}} \right) \times p_{tot} \qquad [atm] \qquad (5)$$

The rate of nitrogen removal can then be related to the nitrogen gas flow rate using the Ideal Gas Law and some constants (with $\underline{N}$ in wt. %, W_{steel} in kg, the molar volume 22.4 Nm^3 $kmole^{-1}$, and nitrogen molecular weight, M_{N2} in kg $kmole^{-1}$):

$$Q_{N_2} = Q_{CO} \times \left(\frac{p_{N_2}}{p_{tot} - p_{N_2}} \right) = -\left(\frac{d\underline{N}}{dt} \right) \times \frac{W_{steel}}{100} \times \frac{22.4}{M_{N_2}} \qquad \left[Nm^3 / s \right] \qquad (6)$$

During the rise of the bubble, the nitrogen partial pressure inside the bubble does not necessarily reach equilibrium with the nitrogen content in the steel; there are kinetic constraints to be discussed in Chapter 5. Therefore, it is convenient to define the gas efficiency for nitrogen removal as the extent of attainment of equilibrium: $p_{N_2} = h_{CO}^{N_2} \times p_{N_2}^{eq}$. This term can then be introduced into the expression for the nitrogen removal rate:

$$\left(\frac{d\underline{N}}{dt} \right) = -\left(\frac{h_{CO}^{N_2} \times p_{N_2}^{eq}}{p_{tot} - h_{CO}^{N_2} \times p_{N_2}^{eq}} \right) \times \frac{Q_{CO} \times 100}{W_{steel}} \times \frac{M_{N_2}}{22.4} \qquad \left[wt.\ \% / s \right] \qquad (7)$$

Rearranging the equilibrium relationship for Sievert's law and introducing the activity coefficient for nitrogen, f_N yields:

$$\underline{N} = \left(\frac{K_N}{f_N} \right) \times \sqrt{p_{N_2}^{eq}} \qquad \left[wt.\ \% \right] \qquad (8)$$

which can be introduced into eq. (7), along with a constant: $a = \frac{100}{W_{steel}} \times \frac{M_{N_2}}{22.4}$, $\mathrm{Nm^{-3}}$:

$$\left(\frac{d\underline{N}}{dt} \right) = -a \times Q_{CO} \times \left(\frac{h_{CO}^{N_2} \times \frac{f_N^2 \times \underline{N}^2}{K_N^2}}{p_{tot} - h_{CO}^{N_2} \times \frac{f_N^2 \times \underline{N}^2}{K_N^2}} \right) = -a \times Q_{CO} \times \left(\frac{h_{CO}^{N_2} \times f_N^2 \times \underline{N}^2}{p_{tot} \times K_N^2 - h_{CO}^{N_2} \times f_N^2 \times \underline{N}^2} \right)$$

$$\left[wt.\ \% / s \right] \qquad (9)$$

The final step is to integrate eq. (9) by separating the independent variables $\underline{N}$ and t to that the time can be calculated to remove nitrogen from $\underline{N}_i$ to $\underline{N}_f$:

$$\Delta t \times a \times Q_{CO} = -\int_{\underline{N}_i}^{\underline{N}_f} \left(\frac{p_{tot} \times K_N^2 - h_{CO}^{N_2} \times f_N^2 \times \underline{N}^2}{h_{CO}^{N_2} \times f_N^2 \times \underline{N}^2} \right) \times d\underline{N} \qquad [-] \qquad (10)$$

Another important parameter is the carrier gas consumption per tonne of steel, $V_{CO} = \left(\frac{Q_{CO} \times 1000}{W_{steel}} \right) \times \Delta t$, $\mathrm{Nm^3\ tonne^{-1}}$, which can then be directly related to the change in nitrogen content in the steel:

$$V_{CO} = -\frac{1000}{a \times W_{steel}} \times \left(\int_{\underline{N}_i}^{\underline{N}_f} \frac{K_N^2 \times p_{tot} \times d\underline{N}}{h_{CO}^{N_2} \times f_N^2 \times \underline{N}^2} - \int_{\underline{N}_i}^{\underline{N}_f} d\underline{N} \right) = \frac{1000}{a \times W_{steel}} \times \left\{ \left[\frac{K_N^2 \times p_{tot}}{h_{CO}^{N_2} \times f_N^2} \times \left(\frac{1}{\underline{N}_f} - \frac{1}{\underline{N}_i} \right) \right] - \right.$$

$$\left. -\left(\underline{N}_i - \underline{N}_f \right) \right\} \qquad \left[Nm^3 \ tonne^{-1} \right] \qquad (11)$$

The constants on the right hand side of eq. (11) can be simplified as $\frac{1000}{a \times W_{steel}} = \frac{W_{steel}}{100} \times \frac{22.4}{M_{N_2}} \times \frac{1000}{W_{steel}} = \frac{224}{M_{N_2}}$, $kg \times \frac{\frac{Nm^3}{kmole}}{\frac{kg}{kmole}} \times \frac{\frac{kg}{t}}{kg} = Nm^3 \ tonne^{-1}$, so that the carrier gas volume expression reduces to:

$$V_{CO} = \left(\frac{224}{M_{N_2}} \right) \times \left[\frac{K_N^2 \times p_{tot}}{h_{CO}^{N_2} \times f_N^2} \times \left(\frac{1}{\underline{N}_f} - \frac{1}{\underline{N}_i} \right) - \left(\underline{N}_i - \underline{N}_f \right) \right] \qquad \left[Nm^3 \ tonne^{-1} \right] \qquad (12)$$

This equation is widely used in the literature for the carrier gas consumption with appropriate selections for K_N, $h_{CO}^{N_2}$, and f_N. These quantities may change over the course of the injection, but have been considered to be constants in the integration procedure. The changes have lead investigators to make convenient approximations; *e*.g. Yavoiskii [21] found that the carrier gas efficiency could be considered to decrease from about 0.93 at the start of injection to 0.7 at the end.

In order to determine the final nitrogen content for any given gas consumption, equation (12) can be re-arranged:

$$V_{CO} \times \frac{M_{N_2}}{224} = \left[\frac{K_N^2 \times p_{tot}}{h_{CO}^{N_2} \times f_N^2} \times \left(\frac{\underline{N}_i - \underline{N}_f}{\underline{N}_i \times \underline{N}_f} \right) - \left(\underline{N}_i - \underline{N}_f \right) \right] \qquad [-] \qquad (13)$$

Introducing two parameters $b = V_{CO} \times \frac{M_{N_2} (= 28)}{224}$, and $g = \frac{K_N^2 \times p_{tot}}{h_{CO}^{N_2} \times f_N^2}$, eq. (13) becomes:

$$g \times \left(\underline{N}_i - \underline{N}_f \right) - \underline{N}_i \times \underline{N}_f \times \left(\underline{N}_i - \underline{N}_f \right) - b \times \underline{N}_i \times \underline{N}_f = 0 \qquad [-] \qquad (14)$$

that can be further rearranged to a quadratic equation in $\underline{N}_f$:

$$\underline{N}_i \times \underline{N}_f^2 - \left(\underline{N}_i^2 + b \times \underline{N}_i + g \right) \times \underline{N}_f + g \times \underline{N}_i = 0 \qquad [-] \qquad (15)$$

The final nitrogen is then the positive root of the quadratic equation:

$$\underline{N}_f = \frac{\left(\underline{N}_i^2 + b \times \underline{N}_i + g\right) - \sqrt{\left(\underline{N}_i^2 + b \times \underline{N}_i + g\right)^2 - 4 \times g \times \underline{N}_i^2}}{2 \times \underline{N}_i} \qquad \left[wt.\ \%\right] \qquad (16)$$

The quadratic equation is rather cumbersome to use, but a convenient approximation can be used. The difference $\left(\underline{N}_i - \underline{N}_f\right)$ in eq. (12) is small compared to the other terms, and can be neglected. It is also convenient to define another term $d = \left(\frac{224}{M_{N_2}}\right) \times \frac{K_N^2 \times p_{tot}}{h_{CO}^{N_2} \times f_N^2} \times \frac{1}{\underline{N}_i}$, Nm^3. This results in a very simple form between the change in nitrogen content and the required carrier gas volume:

$$V_{CO} = d \times \left(\frac{\underline{N}_i}{\underline{N}_f} - 1\right) \qquad \left[Nm^3\right] \qquad (17)$$

This equation can be rearranged to solve for $\underline{N}_f$:

$$\underline{N}_f \times \left(1 + \frac{d}{V_{CO}}\right) - \underline{N}_i \times \frac{d}{V_{CO}} = 0 \qquad [-] \qquad (18)$$

and finally yields:

$$\underline{N}_f = \underline{N}_i \times \frac{d}{d + V_{CO}} \qquad \left[wt.\ \%\right] \qquad (19)$$

It is clear that very good nitrogen removal will result for $V_{CO} >> d$. The extent of nitrogen removal or the nitrogen removal efficiency can be defined and related to eq. (20) in the form:

$$h_{N2} = \left(\frac{\underline{N}_i - \underline{N}_f}{\underline{N}_i}\right) = \frac{V_{CO}}{d + V_{CO}} \qquad [-] \qquad (20)$$

The simplification following eq. (16) has a negligible effect on the accuracy of calculations. This is demonstrated by comparing $\underline{N}_f$ from eq. (19) with that from eq. (16) and then substituting them into eq. (20). The results are plotted in Figure 7 for two values of $h_{CO}^{N_2}$. The two curves cannot be distinguished from one another in the diagram, showing that the simplification is appropriate.

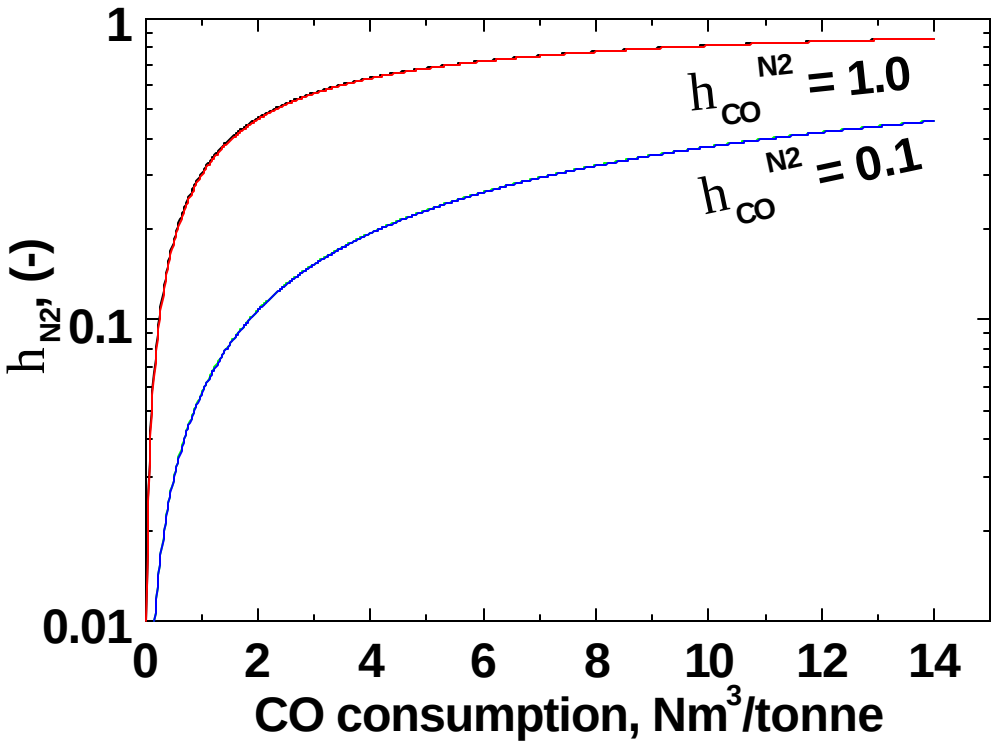

Figure 7. The extent of nitrogen removal as a function of CO consumption for two values of the extent of saturation of the gas with nitrogen, $h_{CO}^{N_2}$, 0.1 and 1.0 for 100 ppm initial nitrogen in steel. Note that the exact solution and the simplified solution fall on the same line for each case.

3. 2. Early experiments at North Star Steel

Diagrams such as Figure 7 are useful for understanding the thermodynamic limits of industrial processes. The data from North Star Steel [2, 7 – 11] is plotted in this manner in Figure 8. The lines were calculated for average conditions (1.5 atm total pressure, 82 ppm N and 1600°C). The value for d was taken as 3.19 Nm^3 tonne^{-1}. The line for $h_{CO}^{N_2} = 1$ corresponds to saturation of the bubble with nitrogen, and is the best possible case. Most of the data falls between that line and 10% saturation ($h_{CO}^{N_2} = 0.1$).

In these experiments iron carbide and DRI was added to heats of AISI 1018 heats. There were 36 experimental heats in four conditions:

- iron carbide (5 heats)
- conventional C – O boil (23 heats)
- 5% DRI charge (5 heats), and
- high sulfur operation (3 heats).

The spread in the data is due to kinetic factors, and scatter in the data. The regions of "Low Efficiency" and "Expensive Process" are subjective at this point. The "Economic Range" corresponds to a DRI addition that depends on material quality (for example, 5.4 % addition to

steel generating 0.06 Nm^3 $tonne^{-1}$ DRI to remove approximately a half of the nitrogen from the steel), for which the injection conditions differ for each plant.

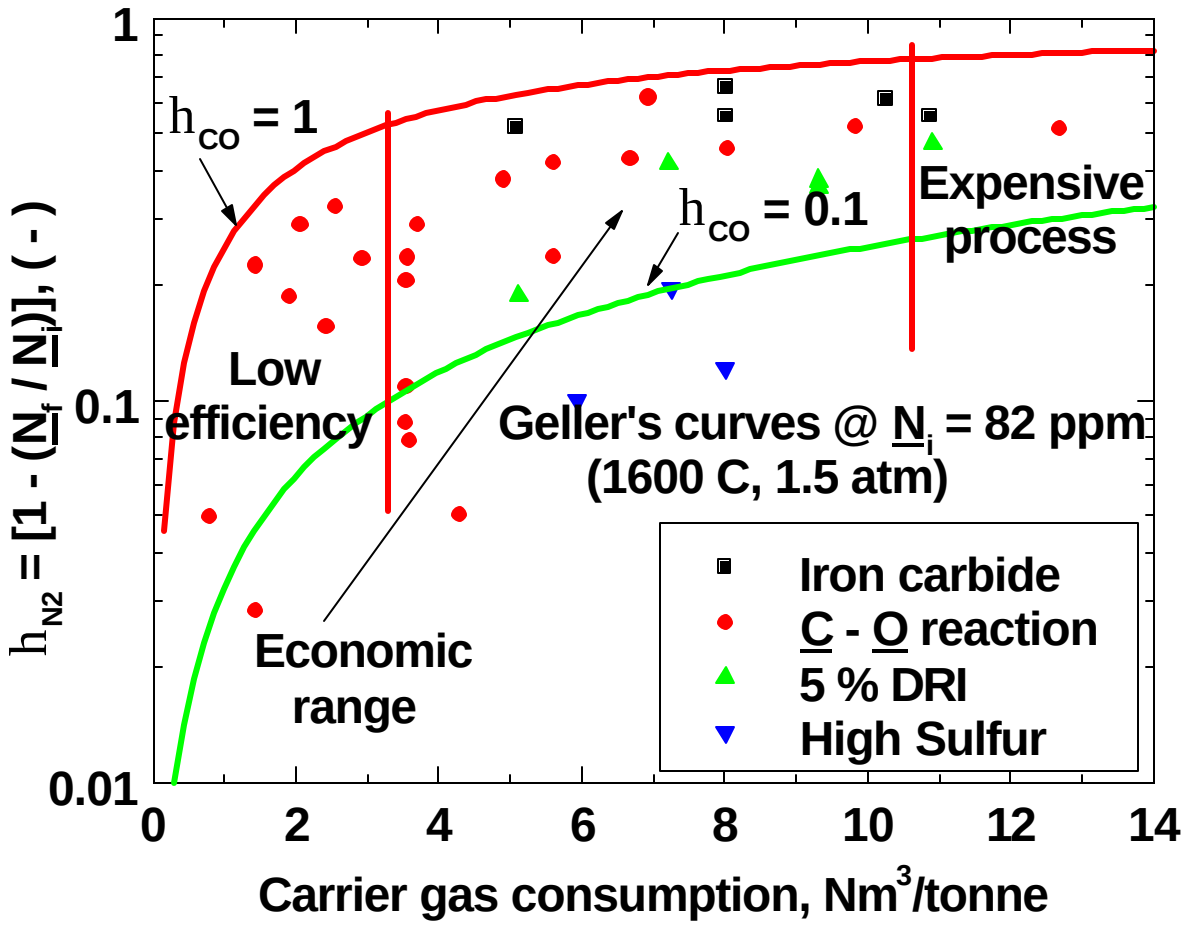

Figure 8. Influence of CO carrier gas consumption on nitrogen removal, re-plotted from North tar data [7, 15, 17]).

3. 3. Recent Industrial Data from Ispat Hamburger Stahlwerke

Approximately 2500 heats from Ispat Hamburger were analyzed to determine if DRI fines reduce the nitrogen. The final tap nitrogen for heats with DRI lumps and DRI lumps + fines were 46 and 41 ppm, respectively, indicating there is some extra removal due to the fines, *i.e.* more than dilution.

Our understanding of the Ispat Hamburger operations comes from Mike Lowry, summarized from the conference call on April 3rd, 2003 as follows: They collect the fines from their Midrex plant and inject them into the EAF to dispose of them. On the heats that they inject in their 135 tonne furnace, they usually inject 10 tonnes, but could be up to 20 tonnes. The fines are injected

while the DRI is being belt fed. The fines injection rate is 1.5 tonnes minute^{-1} and the total DRI feed (belt + injection) is between 3.3 and 4.8 tonnes minute^{-1}. The scrap to DRI rate varies from heat-to- heat. Their primary concern is to keep the level of residuals (Cu, etc.) low while using scrap that can be quite variable.

The data that was supplied was collected between January 2nd 2003 and April 27th 2003. The following is our interpretation of their data.

They have 6 different conditions for their charges:

- Scrap-based, with commercial scrap;
- Scrap containing commercial and internal recycling materials + DRI lumps ("rescued heats");
- Commercial scrap + DRI lumps only;
- Commercial scrap + DRI mix (lumps + fines), 100 % DRI lumps, and
- 100 % DRI mix (lumps + fines).

Unfortunately, there is no condition that exactly suits the needs of our project: scrap + DRI fines. Therefore, we must resort to comparing 3 and 4 from as below.

Table IX shows the distribution of the heats in the 6 conditions. We decided not to use "turned-around" and other unusable heats that only amounted to 14 out of the 2518 heats, so we were left with 2504 heats to analyze. It is clear that 85% of the heats are scrap + DRI lumps (condition 3), and about 9% are scrap + DRI mix (condition 4). We will also ignore the 12 "rescued" heats since we are not certain what happened with them.

Table X shows the Tap Nitrogen for the various conditions. The use of 100 % commercial scrap leads to high nitrogen (68 ppm). Mixing scrap with DRI lumps is certainly beneficial, dropping the nitrogen down to 46 ppm (condition 3). It is most significant for our project that for condition 4 (scrap + DRI mix) the average was 41 ppm. The fines amounted to 3 to 14% of the charge for condition 4. With 100% DRI charge the nitrogen level was the lowest: 20 ppm. It is very difficult to be more quantitative about the differences with the fines because we do not know the "starting" nitrogen in these heats. Nevertheless, it is encouraging that the fines do reduce the nitrogen levels.

Most of the effects of DRI on nitrogen removal are attributed to the "dilution effect", *i.e.*, the DRI contains less nitrogen than scrap. This is certainly true for the present data, and is illustrated with the following simple calculation. In this calculation we ignore the effects of both the melting conversion ratio and the hot heel amount. We assume that 100% scrap produces heats with 68 ppm N and 100% DRI produces 20 ppm N, according to Table X. The linear interpolation of this is plotted as the "DRI dilution line" in Figure 9. A linear regression on the same data, using Matlab produces the "Matlab fitline". The lines are very close together, indicating that the dilution effect is primarily responsible for the reduction in nitrogen.

Table IX. Types of DRI use data at Ispat Hamburger (* - zero nitrogen) (** – no DRI used here) (*** - incident involving the yield) (**** – over-saturation values) (***** - "rescued" steel weight).

#	Heat Parameter/Batch Structure	Scrap (commercial only)	Scrap + DRI lumps "rescued"	Scrap + DRI lumps	Scrap + DRI mix	100 % DRI lumps	100 % DRI mix
1.	Total: 2518 (100 %)	36 (1.43 %)	20 (0.79 %)	2119 (84.16 %)	235 (9.33 %)	100 (3.97 %)	8 (0.32 %)
2.	Turned-around: 6 (0.24 % of total)	0	6	0	0	0	0
3.	Unusable data: 8 (0.32 % of total)	0	1* + 1**	1*** + 3****	0	2*****	0
4.	Effective: 2504 (99.44 % of total)	**36**	**12**	**2115**	**235**	**98**	**8**

Table X. Tap Nitrogen Data for the 6 charging conditions.

	Condition	Average of Tap Nitrogen, ppm	Standard Deviation of Tap Nitrogen, ppm
1.	100 % commercial scrap	68.2 (base – 100 %)	9.0
2.	Commercial scrap + and DRI lumps (rescued heats)	47.2 (30.8 % lower)	13.6
3.	Commercial scrap + variable ratio of DRI lumps	45.8 (32.8 % lower)	17.3
4.	Commercial scrap + variable ratios of both DRI lumps and fines	40.8 (40.2 % lower)	10.1
5.	100 % DRI lumps	20.1 (70.5 % lower)	10.5
6.	100 % DRI lumps + fines	21.3 (68.8 % lower)	8.6

Therefore, the differences that one sees with fines in Table X are probably due to another effect; we submit that it is the rinsing effects of the evolved CO.

The biggest difficulties in analyzing the present data are the facts that fines are injected at different DRI lump consumption and scrap contains various nitrogen contents. Based on this analysis, we believe that the injection of DRI fines can provide a good removal without massive DRI consumption. To prove this, more detailed plant information is needed.

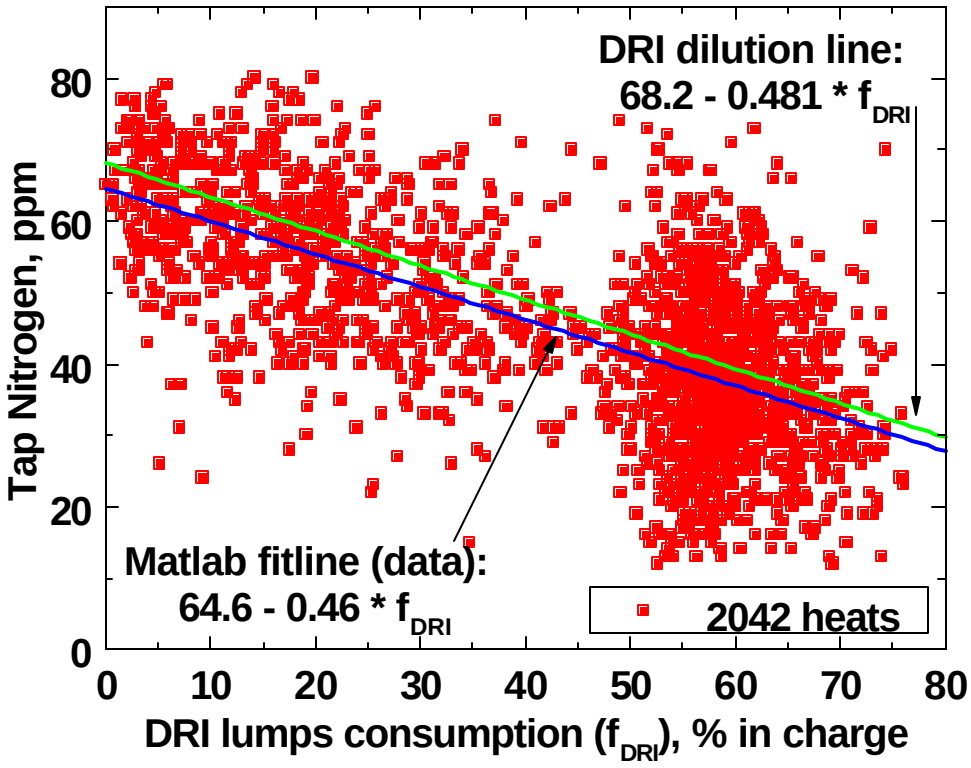

Figure 9. Effect of DRI lump use on Tap Nitrogen, based on the dilution effect.

3.4. BHP Research on Iron Carbide

A paper published during our program reporting pilot trials carried out at BHP Research Center in Australia confirmed that iron carbide fines injected into the liquid steel could remove the nitrogen [22]. Although in terms of experimental performance (including top and bottom injection) it was a clear success; the conditions that they used (higher nitrogen content, high carrier gas (Ar), and the lower gas generation capability because of unbalanced C and O and high pneumatic conveying gas rate) make it difficult to extrapolate to DRI conditions.

4. PILOT SCALE INJECTION TRIALS

The original plan called for pilot scale injection of DRI fines into 60-kg heats of steel melted in an induction furnace, so that the key operational parameters could be understood. Unfortunately, none of the injections worked. The apparatus is shown in Figure 10.

Flowability tests in which the fines were injected into a bin instead of liquid steel worked well. The major problem was lance clogging shortly after injection into the steel started. Seven heats with multiple injection trials in each heat were attempted. To overcome the problems different particle sizes, lance diameters, solids feeding rates, conveying gas rates were tested, and the motor on the screw feeder was changed; all to no avail. This is the first time that we have not been able to successfully inject in our injection projects. It should be noted that solids injection is easier to conduct on the full-scale as Hamburger Stahlwerke has been doing for many years.

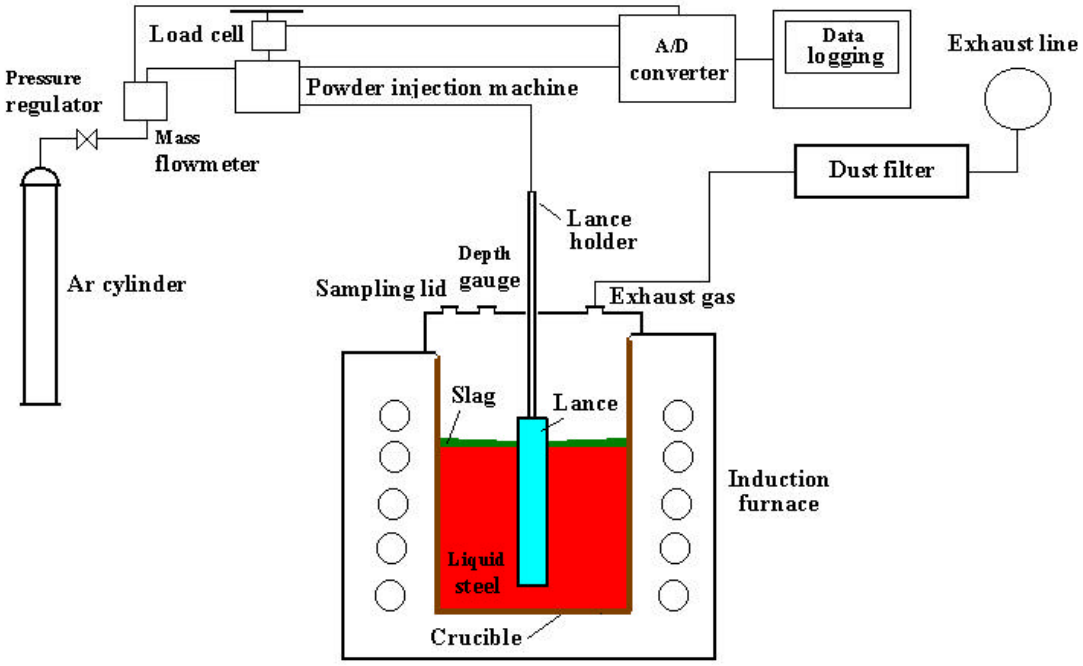

Figure 10. Schematic diagram of the pilot plant apparatus for DRI powder injection.

A conference call was held with industrial sponsors and AISI staff, when it was decided to discontinue the induction furnace trials. The feasibility of full-scale trials with one of the partners was proposed, but it was not possible to arrange the trials.

5. KINETIC MODEL

The overall structure of the kinetic model is shown schematically in Figure 11. The model requires input on the characteristics of the DRI that have been developed through the DRI Characterization in Chapter 2. Inputs of the operational conditions (*e.g.* DRI feed rate, lance submergence, bath temperature and composition, and the liquid pool size) are also required.

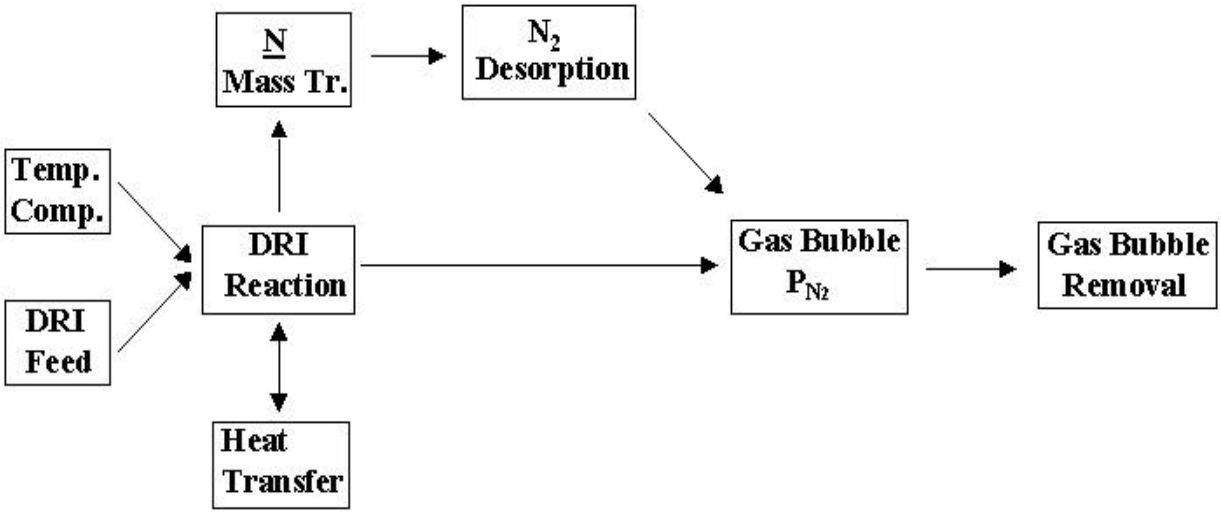

Figure 11. Overall structure of the kinetic model for nitrogen de-sorption using DRI fines injection.

Heat transfer to the injected DRI fines is unlikely to be rate controlling. In Chapter 2 it was shown that the DRI particles start to internally react at approximately 500 °C, and potentially could start to react in the injection lance. However, calculations based on the work of Irons [23], show that particle preheating inside the lance is very limited in industrial conditions. Furthermore, once the particles contact the liquid steel they will react almost instantaneously to release CO because they are so small [24].

This Chapter examines the kinetic constraints to transfer of nitrogen from the steel to the rising bubbles. The major assumptions underlying the calculations are:

- Mass transport control is on the liquid side of the interface; diffusion in the bubble is much faster
- The rate of mass transport may be reduced by adsorption of sulphur and oxygen at the interface
- The transport of nitrogen from the bulk of the liquid (bulk mixing) to the boundary layer around the interface is not rate limiting, as has been found for all powder injection processes [24].

Further assumptions and details of the model are contained in *Appendix 5*. The model is briefly described in this Chapter, and developed in stages. In the first stage, the effects of sulphur and

oxygen on the transfer are ignored, and then included. Figure 12 shows the concentration profiles in the vicinity of the interface; according to the above assumptions there are no gradients in the gas phase, and the interfacial liquid concentration is in equilibrium with the gas phase.

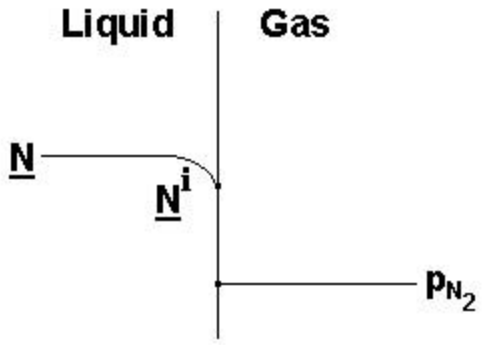

Figure 12. Model of nitrogen transfer from liquid steel to the gas bubble.

This first stage of development of the model considers only a single bubble, so it is assumed that the nitrogen content in the steel remains constant during the rise. The model is based on developing differential equations for the number of moles of nitrogen transferred, the nitrogen content in the bubble and the bubble diameter. The details are presented in *Appendix 5*.

The number of moles transferred is based on using a mass transfer coefficient for small bubbles that depends on diameter. It is convenient to use the bubble rising distance, y, as the independent variable, rather than time, so that the mass transfer expression becomes:

$$\frac{dn_{N_2}}{dy} = \frac{k_N \times A_B}{U_B} \times \frac{r}{2800} \times \left(\underline{N} - \underline{N}_{eq} \right) \qquad [kmoles/m] \qquad (21)$$

The equation becomes more complicated with the substitution of expressions for the mass transfer coefficient, and the pressure dependent equilibrium nitrogen content:

$$\frac{dn_{N_2}}{dy} = \sqrt{\frac{D_N \times p \times d_B^3}{U_B}} \times \frac{r}{1400} \times \left\{ \underline{N} - K_N \times \sqrt{\frac{\left[p_A + r \times g \times (H - y) + \frac{4 \times s}{d_B} \right] \times \%N_2}{100}} \right\}$$

$$[kmoles/m] \qquad (22)$$

The bubble diameter changes because of the number of moles of nitrogen transferred to the bubble and due to the decreasing pressure as the bubble rises. These phenomena are combined into the expression for the change in bubble diameter during rise:

$$\frac{dd_B}{dy} = \frac{d_B^2 \times \left\langle \left\{ \frac{\frac{dn_{N_2}}{dy}}{n_{CO} + n_{N_2}} \times \left[p_A + r \times g \times (H - y) + \frac{4 \times s}{d_B} \right] \right\} + r \times g \right\rangle}{\left\{ \left[p_A + r \times g \times (H - y) + \frac{4 \times s}{d_B} \right] \times 3 \times d_B \right\} - 4 \times s} \qquad [-] \qquad (23)$$

The nitrogen content of the gas changes because of the mass transfer, but also depends on the initial number of moles of CO present:

$$\frac{d\{\%\ N_2\}}{dy} = \frac{100 \times \frac{dn_{N_2}}{dy} \times n_{CO}}{\left(n_{CO} + n_{N_2}\right)^2} \qquad [vol.\ \% / m] \qquad (24)$$

These differential equations are mathematically stiff; *i.e.* the values change rapidly together. Consequently, they were solved with the appropriate Matlab tools. Typical results are plotted in Figure 13. These calculations show that the bubbles can only pick up a few percent of nitrogen during rise that is a fundamental characteristic of the process. The curves all become parallel after some rise time because the bubbles are approaching the equilibrium nitrogen content with the steel, but the equilibrium content depends on the ferrostatic pressure. The curves are slightly different for each bubble size because of the capillary pressure contribution depends on bubble size; the effect is most pronounced for the 1 mm bubbles. It is also evident that the smaller bubbles reach equilibrium more quickly. These findings have important implications for the proposed process. It is anticipated that very fine bubbles will be produced from the DRI fines, so that they will saturate very quickly, and the bubbles do not need to be produced very deeply in the steel.

The kinetic analysis to this point assumes that the bubble rise does not noticeably change the nitrogen content of the steel; thus, this is essentially a 1-mm "single bubble" analysis. The analysis is now extended to account for the change in nitrogen content of the steel with increased CO consumption. This is done by multiplying the amount of nitrogen removed per bubble by the number of bubbles in a volume of CO. The extent of nitrogen removal, h_{N_2}, can then be calculated, as well as the new nitrogen content in the steel, and the process repeated. The results of this calculation are shown as the points in Figure 14. The results are conveniently plotted as a function of the amount of CO generated (Nm^3 $tonne^{-1}$) that can be converted to the amount of DRI injected. The analysis from the Thermodynamics Chapter is shown for comparison. The comparison shows that the extent of saturation of the bubble with nitrogen, $h_{N_2}^{CO}$, drops off as more gas is injected; *i.e.* it is more difficult to reach equilibrium because of the slow kinetics, and because less nitrogen is present in the steel. It also shows that there is no real difference for the injection depths of 0.1, 0.3 and 0.5 m respectively (Figure 14). This means, the injection depth is only required to provide the uniform distribution of the small CO bubbles. The problem of powder injection will be treated separately in Chapter 6.

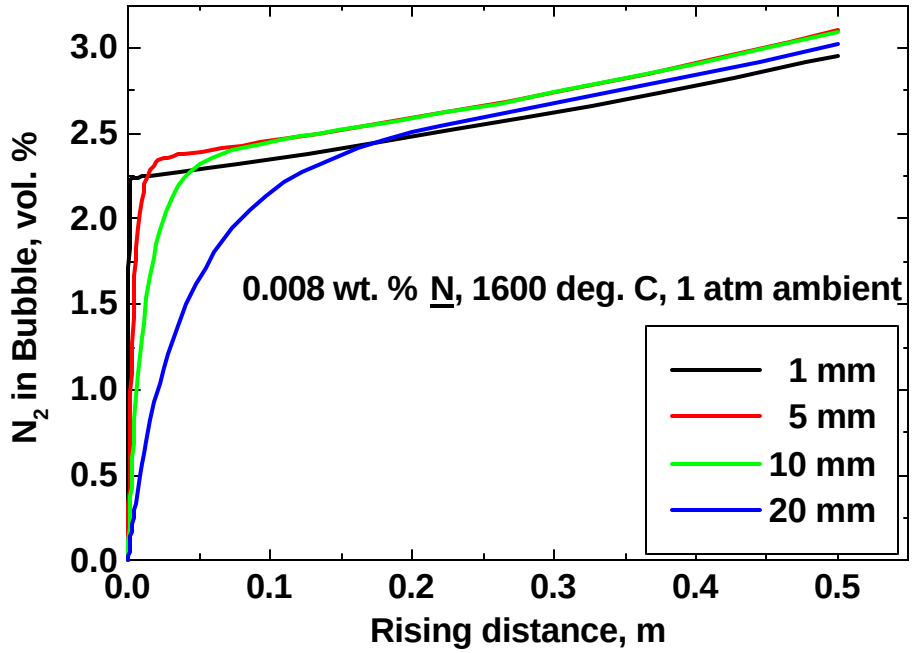

Figure 13. Comparison of nitrogen saturation distances for various bubble sizes.

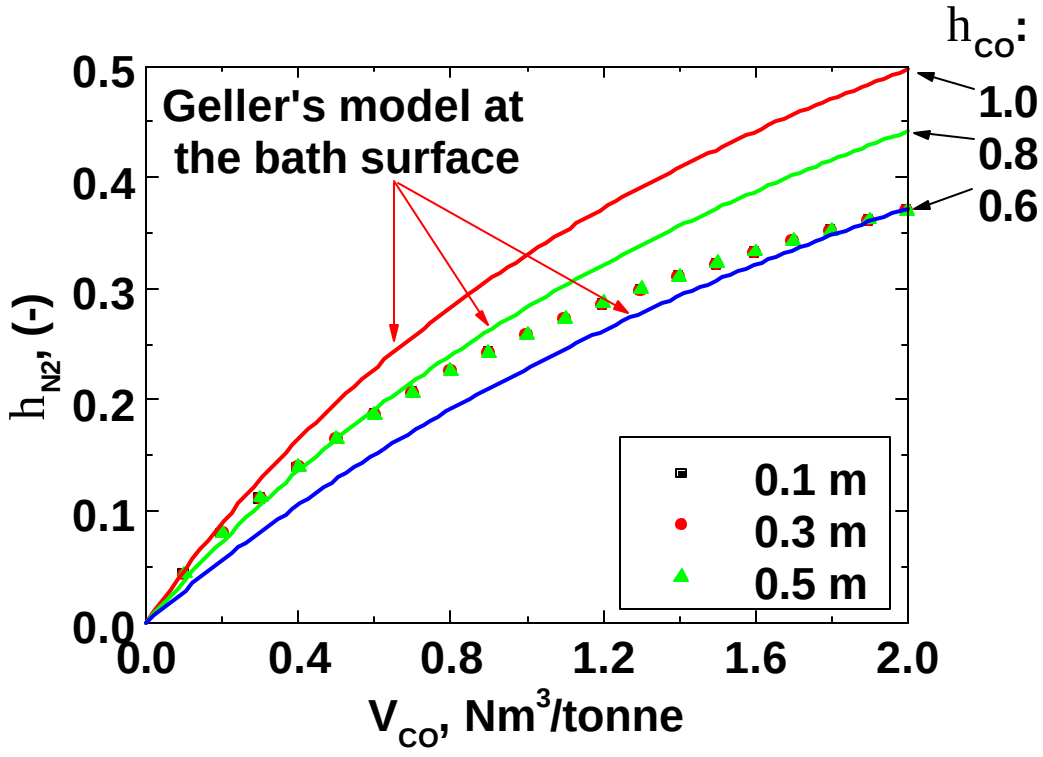

Figure 14. Influence of carrier gas consumption and injection depth on nitrogen removal conditions (base case for initial nitrogen content = 80 ppm, 1600 °C, 1mm CO bubbles) (the corresponding equilibrium curves are indicated).

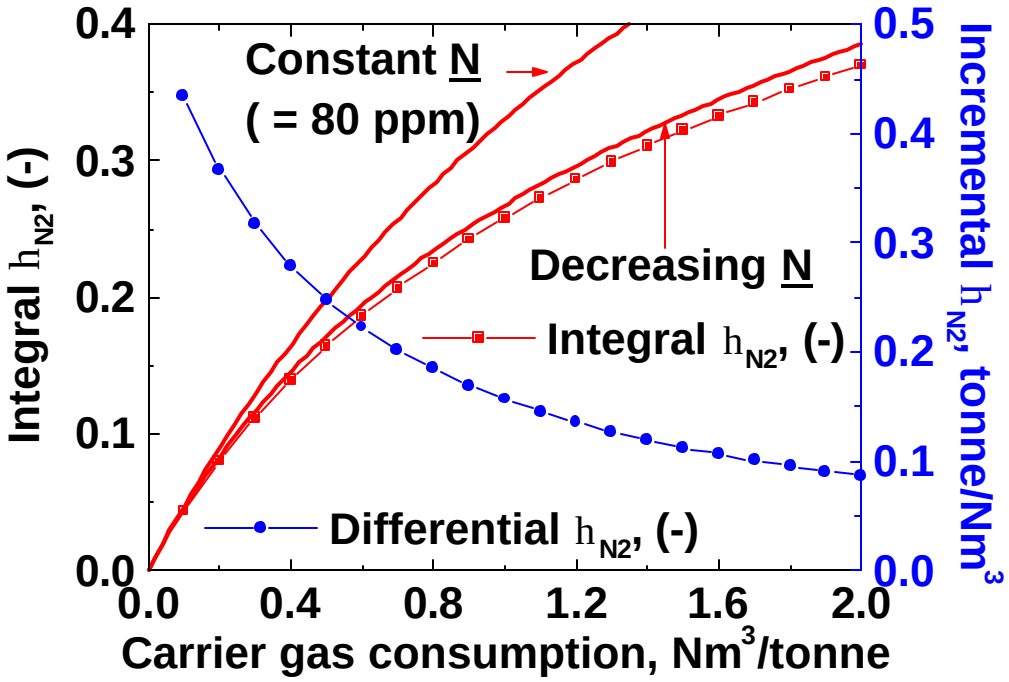

Figure 15. Extent of nitrogen removal with increasing carrier gas consumption for various equilibrium and kinetic conditions.

The kinetic analysis is further extended in Figure 15. The line labeled "Constant N" is the equilibrium extent of nitrogen removal, assuming that the nitrogen content of the steel remains constant, which, of course, is a hypothetical condition. The line labeled "Decreasing N" is also an equilibrium calculation, but the nitrogen content of the steel falls according to how much nitrogen is removed. The line with points adjacent to it is the kinetic calculation (labeled "Integral"), as in Figure 14. The reason that these lines are so close is that the kinetics are rapid, and the bubbles are virtually saturated as much as they can be. This is a convenient finding because the thermodynamic calculations are easier to use. The Integral line shows the overall extent of nitrogen removal for the amount of CO consumed, which is an integral quantity. The "Differential" line shows the extent of removal for each addition quantity of gas, which shows that it is more difficult to remove nitrogen as the nitrogen content decreases in the steel.

It is well-known that nitrogen transfer between steel and gas is impeded by adsorbed oxygen and sulfur at the interface, commonly referred to as chemical control, or when diffusion is also considered as mixed chemical-mass transfer control [25 – 26]. These phenomena are now added to the analysis using data from the comprehensive work of Belton and co-workers [27]. According to the model, oxygen and sulfur occupy surface sites, saturating the interface at only 0.02 % O [26]. Sulfur saturation capacity is according to equation for the chemical reaction rate at the bubble interface, k_C, as established by Byrne and Belton [28]. This equation differs slightly from what would expect from adsorption isotherms [26], but does describe how the nitrogen reaction rate is reduced by oxygen and sulfur (O and S in wt. %, 1580 °C) [29]:

$$k_C^* = r_{c0} \times (1 - \Theta) = \frac{0.0316}{1 + (268 \times \underline{O}) + (134 \times \underline{S})} \qquad \left[m / s / wt.\ \% \right] \qquad (25)$$

The reduction in reaction rate is plotted against $\underline{O} + \underline{S} / 2$, (wt. %) in Figure 16.

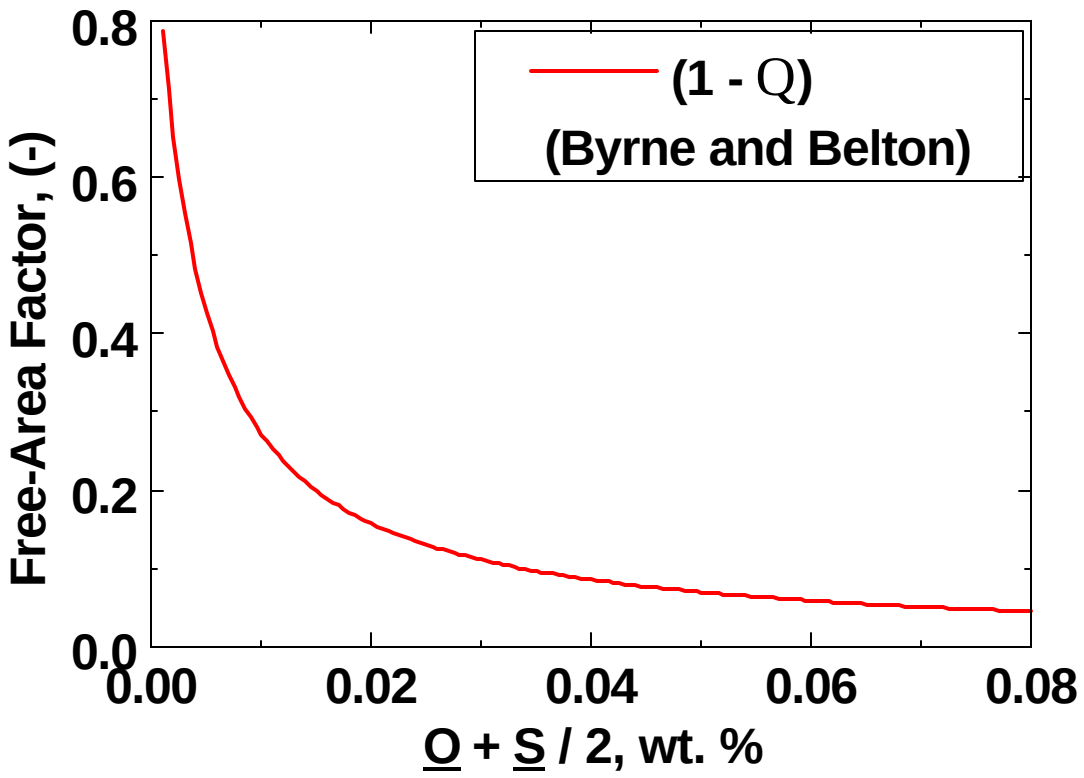

Figure 16. Influence of interfacial coverage on nitrogen transfer regime (adsorption + reaction).

The overall reaction rate considering liquid-phase mass transfer, chemical reaction and gas phase control has been described many times [14, 29 - 30]:

$$\frac{1}{k_{N,\,ov}} = \frac{1}{k_M} + \frac{1}{k_C^* \times \left(\underline{N}_i + K_N \times \sqrt{p_{N_2}} \right)} + \frac{r}{2800} \times \frac{R \times T \times K_N^2}{r_G \times \left(\underline{N}_i + K_N \times \sqrt{p_{N_2}} \right)}$$

$$[s / m] \qquad (26)$$

The plot of eq. (29) in the range of steelmaking interest yields Figure 17. The overall rate is controlled by the "slowest" step. It is clear that the gas phase step is fast, and that the process is mixed liquid-phase mass transfer and chemical control, but mainly chemical control.

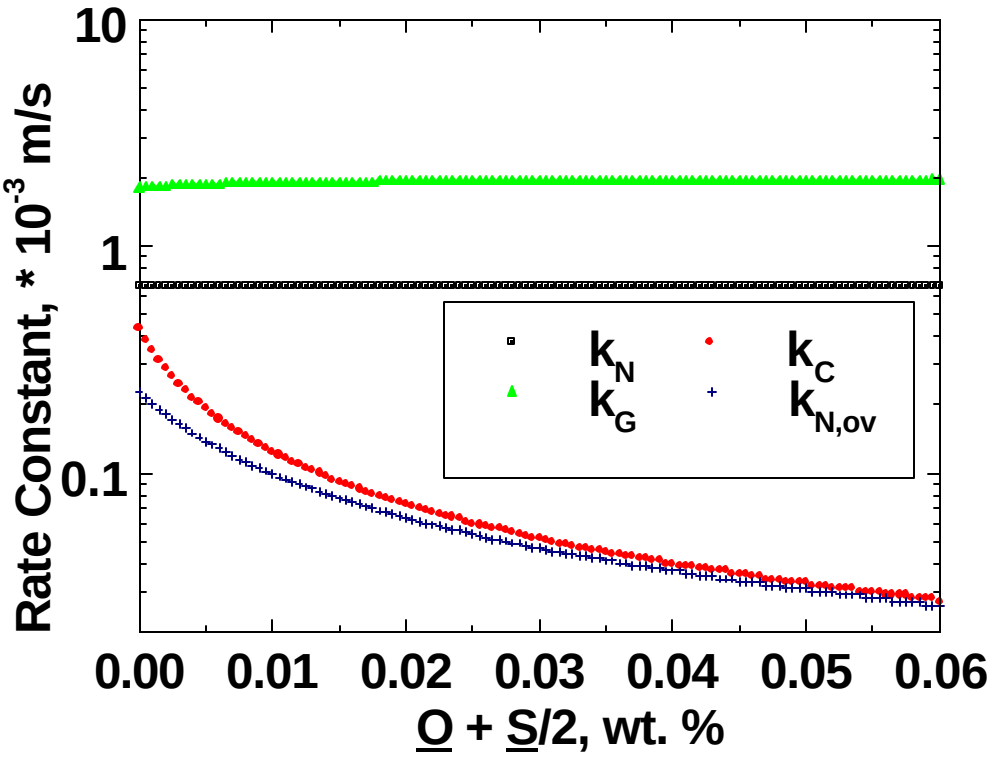

Figure 17. Overall rate constant for nitrogen removal (1580 °C).

If the process is fully controlled by the chemical reaction, then the integration of the second order dependence yields the following expression used in the BHP paper [22]:

$$\left(\frac{1}{\underline{N}_f} - \frac{1}{\underline{N}_i}\right) = \frac{k_C \times A}{V} \times t \qquad [-] \qquad (27)$$

namely there is a straight line relationship between $\left(\frac{1}{\underline{N}_f} - \frac{1}{\underline{N}_i}\right)$ and carrier gas–flushing reaction time. $k_C = k_C^* \times \left(\underline{N}_i + K_N \times \sqrt{p_{N_2}}\right)$.

For a given oxygen activity, if the temperature is increased, the efficiency of nitrogen removal will increase; this aspect will be re-called in Recommendations.

As suggested by the North Star Steel data, high sulfur contents reduce the nitrogen removal rate through the interfacial reaction (Figure 8). It is difficult to apply equation (25) directly to the rate equation because we do not know the exact oxygen, sulfur content and temperature. Therefore a sensitivity analysis was performed; full surface blockage results in a rate 95 % lower, or about 20 times slower. The results of the calculations in Figure 18 show that the bubbles still reach saturation within 20 cm rising distance, even if the rate is 100 times slower than the unblocked surface rate.

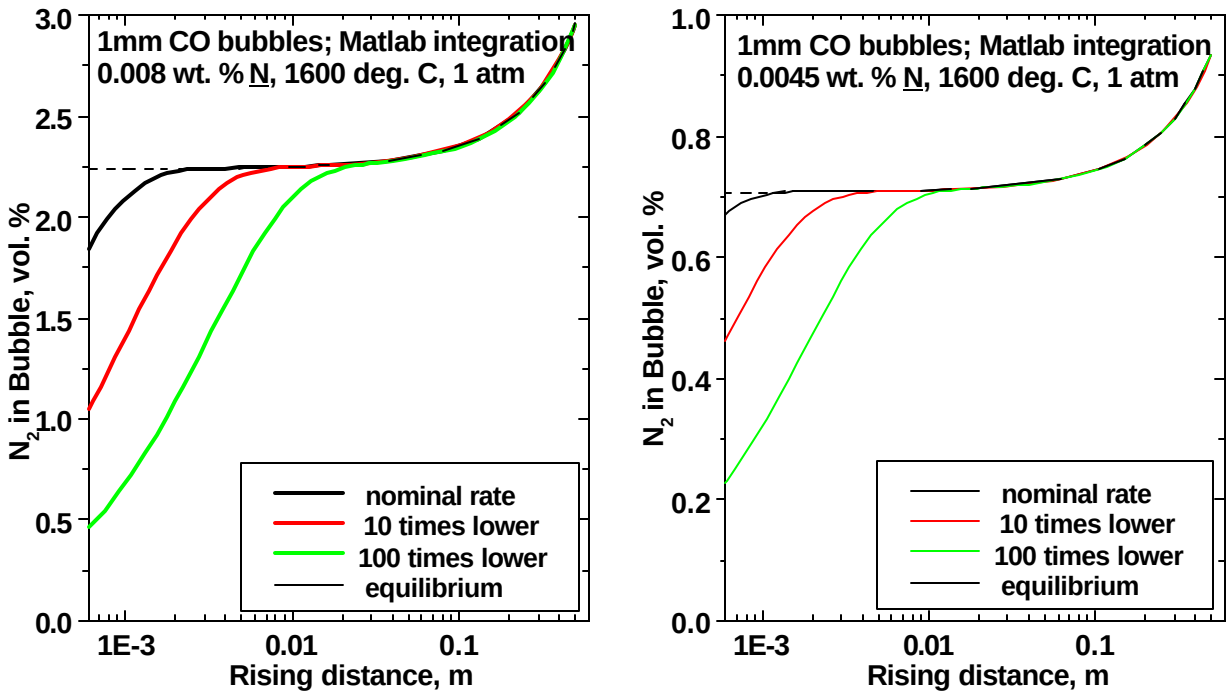

a b

Figure 18. Sensitivity analysis on rate constant:
a – initial nitrogen (80 ppm) ;
b – final nitrogen (45 ppm).

Figure 18 confirms that the nitrogen removal process using the flushing with small CO bubbles cannot be chemically stalled, not even at low final nitrogen contents. This is important as it was shown in Materials Characterization Chapter that the oxygen content in DRI fines may not be balanced by carbon.

6. JET PENETRATION MODEL

6.1. Model description

The final stage of the modeling is the fluid mechanics associated with the injection of the gas and particles. For many years Hamburger Stahlwerke has been injecting DRI fines into the EAF at rates of approximately 1 Tonne min^{-1} [6]. At such high rates, the jets have significant momentum to penetrate into the steel. This is schematically shown in Figure 19.

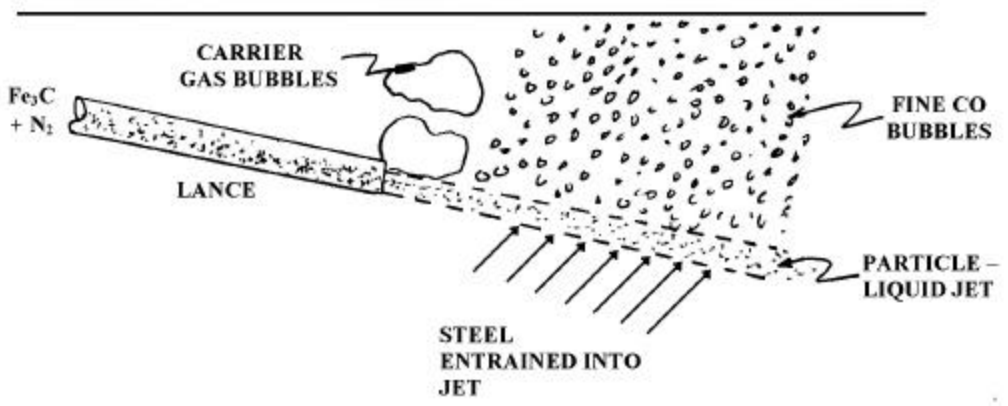

Figure 19. Approach of multiphase development occurring during DRI fines injection through a submerged lance.

Liquid steel is entrained into the jet, and it will expand. The downward momentum of the jet is working against the buoyancy of the jet, and so at some point it starts to rise again. During the jet's descent, the particles are heated by radiation and contact with liquid steel, and start to evolve CO. The large evolution of the fine CO bubbles disrupts the continued jet motion. The modeling of these heat transfer phenomena is beyond our current level of understanding, but it is possible to model the injection in the initial stages. It is useful to do this because the maximum penetration depth and horizontal penetration can be calculated, and matched to a particular EAF configuration. The gas-particle jet penetration model was developed by Gou and Irons [31]. The following major assumptions are employed:

- The flow is assumed to be isothermal.
- The gas and particles have the same velocity in the jet.
- Liquid steel is entrained into the jet, and this is modelled with a constant entrainment coefficient.
- The CO evolved from the DRI, and the particle dissolution, are both ignored.

The nomenclature for the model is shown in Figure 20 in which an inclined jet is shown.

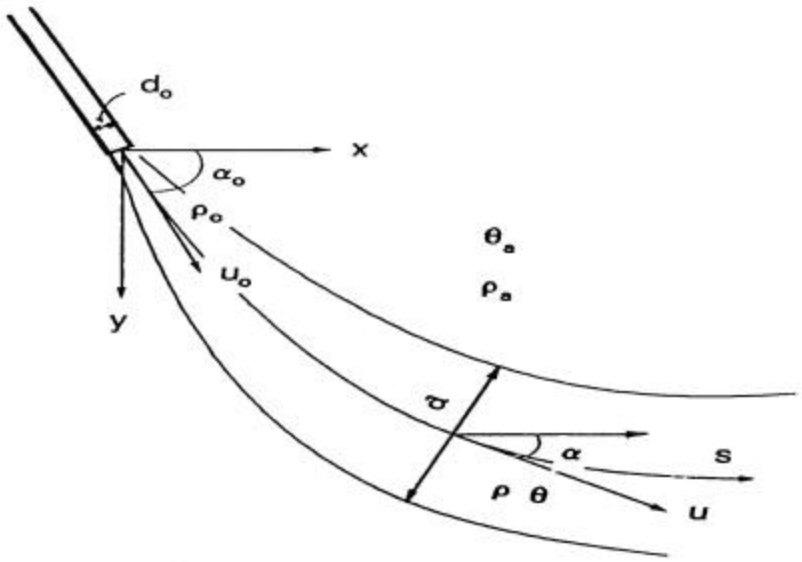

Figure 20. Schematic representation of a jet showing the nomenclature for the model. The jet expands from the lance diameter d_0, to d_j because of entrainment and deceleration of the jet.

Because of the curved trajectory, it is convenient to use distance along the jet axis, *s*, as the space coordinate. Changes along the axis are related to the conventional rectangular coordinates by: $ds = \sqrt{dx^2 + dy^2}$. The model is based on the solution of coupled differential equations for jet velocity, jet diameter, angle and the sum of gas and particle mass fractions [31]:

$$\frac{dU_j}{ds} = -\frac{4 \times k_j \times U_j}{p \times d_j} \times \sqrt{r_r} + \frac{g \times \Delta r_r \times \sin a_j}{U_j} \qquad [s^{-1}] \qquad (28)$$

$$\frac{dd_j}{ds} = \frac{2 \times k_j}{p} \times \left(\sqrt{r_r} + \frac{1}{\sqrt{r_r}} \right) + \frac{g \times d_j \times \sin a_j}{2 \times U_j^2} \times \Delta r_r \qquad [-] \qquad (29)$$

$$\frac{da_j}{ds} = -\frac{g \times \cos a_j}{U_j^2} \times \Delta r_r \qquad [m^{-1}] \qquad (30)$$

$$\frac{dq_j}{ds} = -\frac{4 \times k_j \times q_j}{p \times d_j} \times \sqrt{r_r} \qquad [m^{-1}] \qquad (31)$$

Typical results of the calculation are shown in Figure 21 that show that the jet penetrated 0.81 m vertically from the injection point. It should be noted again that the gas evolution from the DRI will disrupt the jet in the vicinity of this point, and fine CO bubbles will arise vertically from this point. Therefore, the model breaks down at this point and the ascending portion of the jet should be disregarded.

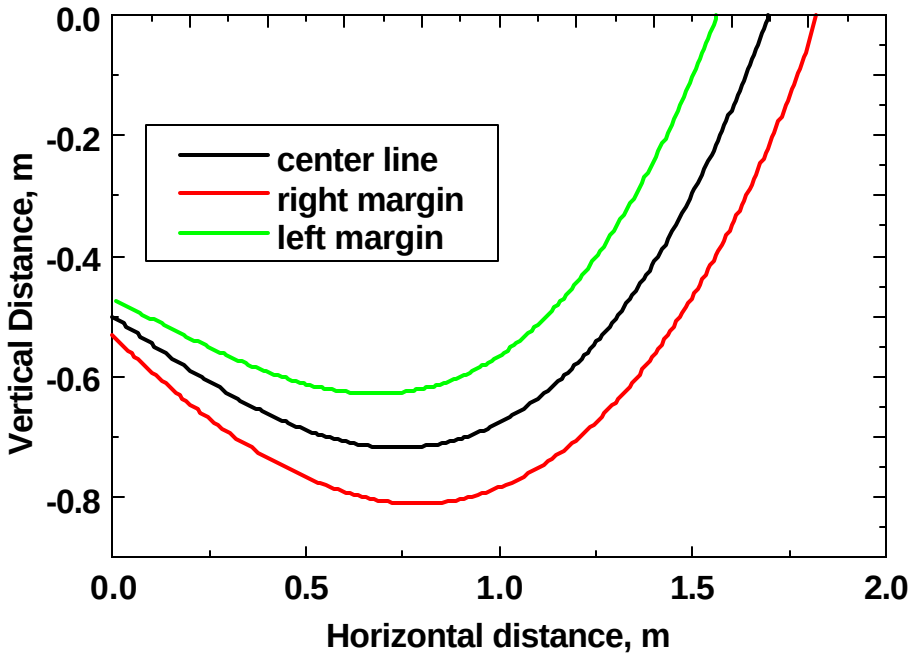

Figure 21. Profile of jet boundaries (inclined lance, ID, 25 degrees angle, 1600 °C, 1020 kg DRI fines min^{-1}, 50 mm lance diameter and 86.6 initial jet velocity) through the steel melt.

To better illustrate the way in which the model can be used to select the injection conditions, particular conditions were used in a typical case. For the calculations Dofasco's 190-tonne capacity furnace was selected, and a 5 % DRI addition in 10 minutes was simulated (*i.e.*, 9500 kg / 10 min = 950 kg min^{-1}).

For these calculations it was assumed that a lance submergence of 0.5 m would be deep enough to ensure high iron recovery from the fines with the substantial dispersion of the particles inside the melt, and it was also assumed that there was a significant liquid pool for injection, such as at 60 % of melting of the charge. For the conditions of Figure 18, this corresponds to about 0.8 m jet penetration depth which is less than the melt-in depth of the 1.26 m.

The sensitivity of the penetration depth to the injection parameters was studied, and reported in the following sections. The parameters were varied in the following manner:

- Lance angle at various lance diameters for a constant powder rate, consequently the jet velocity varies;
- Powder rate at various lance diameters and jet velocities.

The following conditions were considered in addition to the model assumptions:

- The furnace geometry is the 190-Tonne twin-shell EAF at Dofasco Inc. in which the maximum steel bath depth is 1.26 m, and decreases slightly from the furnace centre.
- The lance tip is 0.5 m deep in the steel.
- The top slag is ignored.

- The steel temperature is 1550 °C.
- The carrier gas is air.
- The injection is in the "dense phase" mode in which the solids loading is 100 kg of solid per Nm^3 of carrier gas, yielding a mixture density of 103.8 kg m^{-3}.
- The entrainment coefficient is 0.06.

6.2. Influence of lance angle

Injection with lance internal diameters of 38, 51 and 64 mm (1.5, 2, and 2.5", respectively) were modeled at a constant initial jet velocity of 50 m s^{-1}. This velocity was selected because it is safely above the minimum conveying velocity, but low enough that the conveying pressure and abrasion rates in the line are acceptable. The results of the calculation are shown in Figure 22. Note that the solids rate will increase with the square of the diameter for a constant injection velocity; these rates are shown in the Figure caption.

It can be observed that the injection with the larger lances increases the penetration in both directions, simply because they are bigger. Increasing the lance angle from the horizontal increases the depth of penetration substantially because the jet is more directly opposing the buoyancy effect. However, the horizontal penetration is slightly reduced with increasing angle of injection:

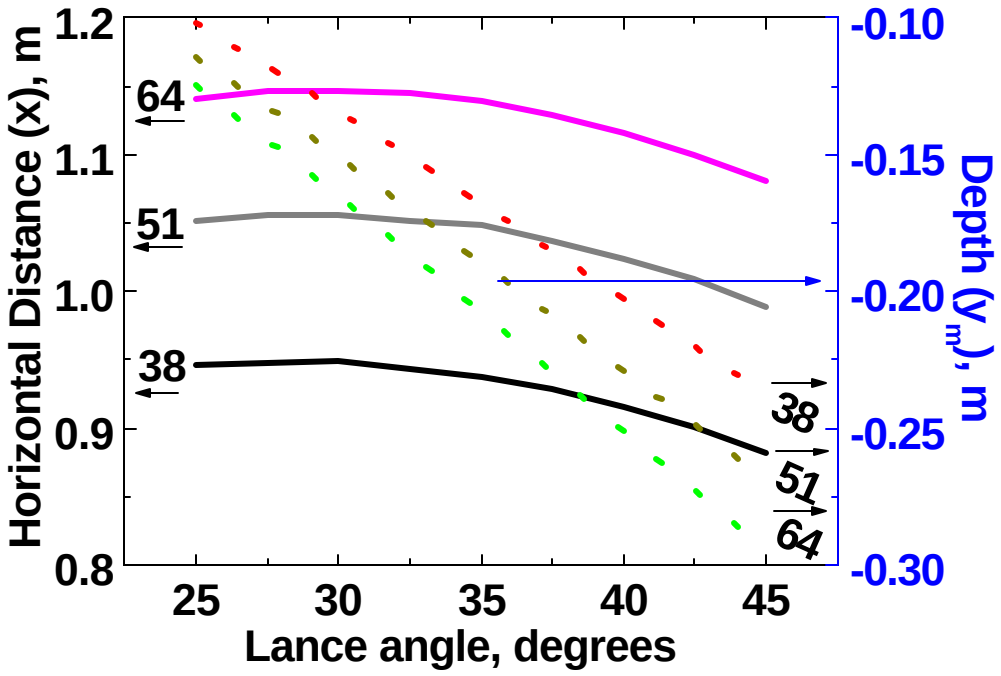

Figure 22. Jet penetration in the steel bath in the horizontal direction (left axix, thick lines) and in depth (right axis, dotted lines). Each lance diameter had a different solids rate:
38 mm – 342 kg min^{-1};
51 mm – 608 kg min^{-1};

64 mm – 950 kg min^{-1}.

6.3. Influence of powder rate

In this set of calculations injection velocities and rates were selected to be in the practical industrial regime. The lance tip was assumed to be 0.5 m below the surface so as to ensure that there are no dust losses. The solid injection rate was chosen to range from 700 to 1400 kg min^{-1} since it is important to inject the DRI fines quickly. The injection velocity was chosen to range from 25 to 100 m s^{-1} because at the low end the particles cannot be conveyed, and at the high end pressure drop and erosion are significant. Because we have selected both the solids rate and the injection velocity, the lance diameter is automatically specified. The diameters are plotted along with the horizontal penetration in Figure 23a. It is clear that the injection velocity has a dramatic effect on the horizontal penetration. The same is true for the penetration depth, shown in Figure 23b. The injection rate, at constant injection velocity, does increase the penetration in both directions, but the effect is much more modest. Therefore, it can be concluded that the most important variables for jet penetration are the injection velocity and angle.

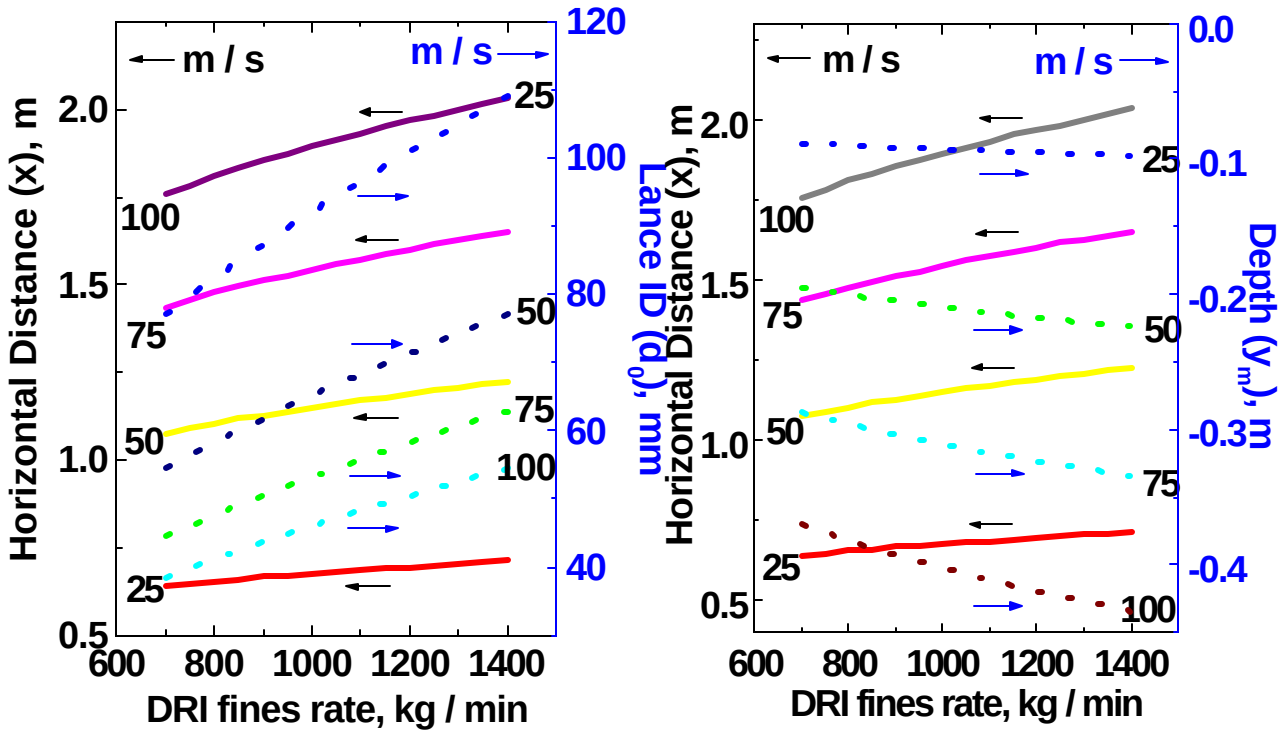

a b

Figure 23. Jet penetration in the steel bath at an injection angle of 35 degrees from the horizontal:
a – horizontal penetration (left axis, thick lines) and lance ID (right axis, dotted lines);
b – vertical penetration .

From the Kinetic modeling in Chapter 5 it was clear that fine CO bubbles saturate with nitrogen from the steel in a very short rising distance, much less that the injection depths calculated in this Chapter. Therefore, the injection rate can be selected according to the amount of DRI required to remove the desired amount of nitrogen and time available in the heat. The angle and location of the injection lance can then be selected so that the jet is in the liquid pool of steel, and does not hit the bottom of the furnace. It is also undesirable to have the CO evolved directly under an electrode since this will generate unnecessary electrical interference. There may be additional logistical constraints on lance position in each furnace.

7. RECOMMENDATIONS

The recommendations that arise from this report fall into three categories:

- The best composition and size of DRI fines to be used;
- The amount of DRI fines required to achieve a specific reduction in nitrogen content in the steel; and
- The injection conditions.

Each one of these will be addressed in the following sections. There is enough information in this report for individual steel companies to make their own techno-economic assessments of the cost of reducing nitrogen with DRI fines injection. These assessments are very site specific regarding the local cost and quality of DRI fines, the economic benefit of reduced nitrogen for the steel products made (or that could be made with lower nitrogen capability), and the availability and cost of the injector and associated lance equipment.

7.1. DRI Composition and Size

The recommendations for this section come from the findings in Chapter 2 (Materials Characterization). Figure 1 shows that the oxygen and carbon contents of the DRI should be balanced to produce CO, and that the contents should be maximized. It is indeed unfortunate that iron carbide materials cannot be produced on an industrial basis since they are superior in this regard.

Steelmakers have long known that DRI with low gangue content is desirable because less energy is required for melting and less slag is generated. This is obviously the case for DRI fines as well. There are a couple of extra considerations for fines injection.

The first issue is that the oxygen content to be considered in Figure 1 is the oxygen content not in the gangue. The second issue is that oxygen in the gangue as oxides will be reduced with carbon in the DRI if it is available. This requires extra energy that is a burden on steelmaking.

There is great variation in what various steel companies consider DRI fines to be. These materials could be the undersize from screening operations in which case the they are generally less than 6 mm (1/4”), or they could be captured in a baghouse, and be much finer. The main restriction on size is that the particles be pneumatically conveyable. In principle, all these sizes should be conveyable on an industrial scale, but test work should verify that this is the case. The suppliers of injection equipment have appropriate test facilities.

The other issue with DRI fines composition is storage and handling. If these materials are left outside, then they will oxidize and pick up moisture. The oxidation will be a source of variability, and may take the composition away from the optimum. The moisture may increase the hydrogen content of the steel. Therefore, the material should be stored in bins, which of course is required for pneumatic conveying.

7.2. DRI Fines Consumption for Nitrogen Removal

These recommendations are a result of the calculations in Chapter 3 (Thermodynamic Analysis) and 5 (Kinetic Model). That work showed that the pick up of nitrogen by mm-size bubbles is very fast, and that equilibrium is essentially achieved in a short rise distance. The major limitation is that the nitrogen content in the bubble is only a few percent. Therefore, CO consumption or generation must be significant.

Summary diagrams have been prepared to show how much CO is required, expressed as Nm^3 $tonne^{-1}$ (Figure 24 a and b). The figure caption shows the calculation to relate that to the gas evolution from the DRI or other material. Four different cases are considered:

Case I

For a CO gas consumption of only 1.0 Nm^3 $tonne^{-1}$, about 25 % of the initial nitrogen can be removed (Figure 8), which is sufficient for some applications. Such condition is reached at 5 % DRI fine addition (or a 1.25 % iron carbide). Comparing Figures 24 a and b, it is clear that it is harder to remove lower nitrogen contents.

Case II

This case considers a CO gas consumption of 2.0 Nm^3 $tonne^{-1}$ that can be achieved with a 10% addition of DRI or a 2.5 % addition of iron carbide.

Case III

This case considers the alternative of carbon injection, at 0.5 % of the heat or 5.0 kg $tonne^{-1}$. It is still assumed that 1-mm bubbles are created, but this is unlikely. Unfortunately, carbon injection will create very large bubbles that will not have the same efficiency as assumed in Figure 24. This is likely the case since charge carbon additions or carbon injection of this magnitude to EAF heats do not remove very much nitrogen from the steel.

Case IV

In this case 5% carbon is assumed to be injected into the heat, which is comparable to the carbon content of blast furnace iron. This is a hypothetical case because large amounts of oxygen would need to be injected as well, and large bubbles would be created. Therefore, it is unlikely that the amount of nitrogen would be removed according to Figure 24.

The other major alternative for nitrogen removal is vacuum degassing. Unfortunately, the kinetics of this process are very slow. For example, the nitrogen content is only decreased from 60 to 30 ppm in a typical process [27, 32]. Moreover, there are additional capital and operating costs for degassing.

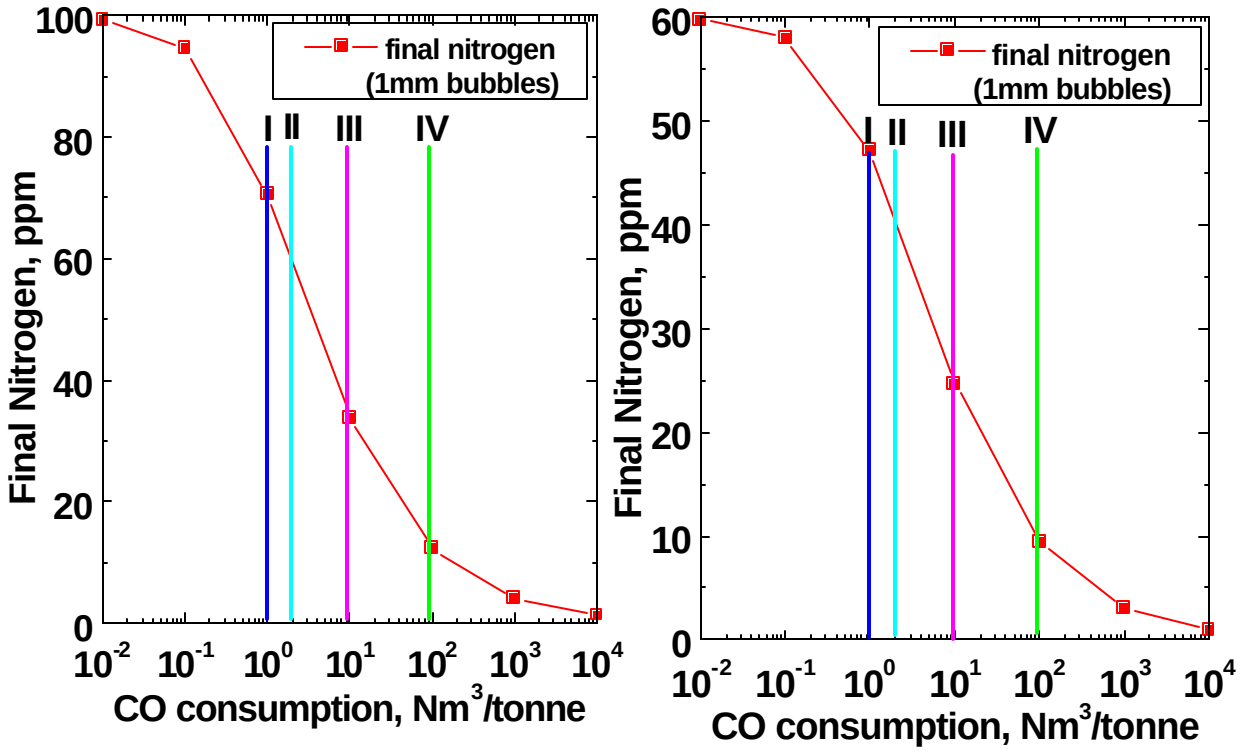

Figure 24. Extent of nitrogen removal for two initial nitrogen concentrations: a – 100 ppm; b – 60 ppm for 0.5 m injection depth at 1600 °C:

I – 5 % commercial DRI or 1.25 % iron carbide in charge, 50 kg tonne^{-1} × 20 Nm^3 tonne DRI $^{-1}$ = 1.0 Nm^3 tonne^{-1}, or 1.25 kg tonne^{-1} × 80 Nm^3 tonne DRI $^{-1}$ = 1.0 Nm^3 tonne^{-1};
II – 10 % commercial DRI or 2.5 % iron carbide in charge, 100 kg tonne^{-1} × 20 Nm^3 tonne DRI $^{-1}$ = 2.0 Nm^3 tonne^{-1}, or 25 kg tonne^{-1} × 80 Nm^3 tonne DRI $^{-1}$ = 2.0 Nm^3 tonne^{-1};
III – carbon injection process – 0.5 % of the batch, 5 kg tonne^{-1} × (22.4 / 12) Nm^3 tonne DRI $^{-1}$ = 9.3 Nm^3 tonne^{-1});
IV – carbon injection process – 5 % of the batch, 50 kg tonne^{-1} × (22.4 / 12) Nm^3 tonne DRI $^{-1}$ = 93.3 Nm^3 tonne^{-1}).

The injection of DRI fines will increase the power requirements for melting. Taking 400 kWh tonne^{-1} as theoretical energy requirement for heating and melting, and the case of a 9500 kg addition to a Dofasco-like furnace, the power required is approximately 2.3 MW (0.95 tonne * 400 kWh tonne^{-1} * 60 / 10 / 1000). It should be noted that the iron in the DRI will reduce the need to melt as much scrap, so the net amount of extra energy will be smaller.

7.3. Injection Conditions

The injection conditions were investigated in Chapter 6 (Jet Penetration Model). It was demonstrated that DRI fines could be injected into heats at rates between 700 and 1400 kg min^{-1}. The major variables that control how far the jet of gas and particles penetrates are the lance

angle and jet velocity. Figures 19 and 20 can be used to select the injection conditions for particular furnaces and production schedules.

8. CONCLUSIONS

The main findings of this study are:

1. The most important characteristics of the DRI fines are the carbon and oxygen contents, and that they be "balanced" to stoichiometrically create CO. Additionally, these quantities should be maximized to create as much CO per tonne of DRI.
2. The gangue constituents of the fines should be minimized so as not to add to the furnace slag volume, but also so that the energy for fayalite reduction is not required.
3. A thermodynamic analysis of the rising effect of CO to remove nitrogen delineated the quantity of CO required to remove specific amounts of nitrogen from steel.
4. A kinetic analysis reveals that for mm-size bubbles, the kinetics are very fast, and the bubbles become saturated with nitrogen in a very short rising distance. Consequently, the fines do not need to be injected very deeply to have the proper effect. Furthermore, the thermodynamic analysis can be used to assess the DRI requirements because the kinetics are fast.
5. Approximately 25 % of nitrogen can be removed from steel with approximately a 5 % addition of DRI fines to an EAF.
6. Analysis of available industrial data from North Star Steel and Hamburger Stahlwerke is consistent with the findings in the thermodynamic and kinetics analyses.
7. A fluid mechanic model for gas-particle jets was adapted to this system, and can be used to select the injection conditions (lance diameter, solids feed rate, solid-to-gas loading and lance angle).

ACKNOWLEDGEMENTS:

The financial assistance from AISI – DOE (award number DE-FC07-97ID13554, Cooperative Agreement # 009) is gratefully acknowledged. The industrial sponsors: American Iron and Steel Institute, Dofasco, Inc., Gallatin Steel Company, Ispat Inland, Inc. Midrex Technologies, Inc., Steel Dynamics, Inc. and Ispat Hamburger Stahlwerke contributed with significant support with samples and technical data. The valuable discussions held with Messrs. Michael Lowry of Ispat Inland and Marco Schünemann of Ispat Hamburger Stahlwerke were very helpful. The authors kindly thank Messrs. Jim Garrett, Martin Van Oosten, Chris Butcher and Frank Gibbs for all experimental support on material characterization.

SYMBOLS:

A_B – bubble interfacial area (= $p \times d_B^2$), m^2;
D_N – nitrogen diffusion coefficient in liquid steel (= 9.0×10^{-9}, at 1600 °C), $m\ s^{-2}$;
DTA – differential temperature between material sample and reference sample, °C (μV);
DTG – incremental mass loss decreasing, s^{-1};
$\underline{E}$ – dissolved element (with subscripts), wt. %;
H – injection depth, m;
K_E - equilibrium constant (e. g. K_N = 0.045 wt. % × $atm^{-1/2}$ at 1600 °C (see *Appendix 1*);
M_{N_2} - molecular mass for nitrogen (= 28), kg $kmole^{-1}$;
Q - gas flow rate (with subscripts for CO and CO_2), $Nm^3\ s^{-1}$;
R – ideal gas constant, 8.314 J $kmole^{-1}\ K^{-1}$;
R_G - gas volume, Nl kg^{-1} DRI;
T – absolute temperature, K;
TG – fractional mass loss decreasing, (-);
U_B - CO bubble velocity, $m\ s^{-1}$;
U_j - jet (carrier gas + DRI fines) velocity, $m\ s^{-1}$;
V – bubble volume (also V_0, at t = 0 or y = 0), m^3;
V_{CO} – CO consumption (= $r_G \times Q_{DRI} \times t$), Nm^3 $tonne^{-1}$;
W_L - mass loss for DRI particle, %;
W_{steel} - liquid steel mass, kg;
d_B - bubble diameter, mm;
d_p - DRI particle diameter, μm;
d_0 - jet (carrier gas + DRI particles) diameter (also, d_j), m;
f - efficiency of nitrogen de-sorption, [29], (-);
f_{DRI} - fraction of DRI fines, % in charge;
f_N - nitrogen activity coefficient, (-);
g - gravitational acceleration, $m\ s^{-2}$;
k_C - chemical reaction rate at the bubble interface (nitrogen de-sorption), $m\ s^{-1}$;
k_C^* - same, percentage-incremental value, $m\ s^{-1}$ wt. $\%^{-1}$;
k_G - gas phase mass transfer coefficient (nitrogen), $m\ s^{-1}$;
k_j - entrainment coefficient of the liquid steel due to jet (carrier gas + DRI particles), [31], (-);
k_G - liquid phase mass transfer coefficient (nitrogen), $m\ s^{-1}$;
k_M - nitrogen mass transfer coefficient (with scripts), $m\ s^{-1}$;
n - reacting specie amount (with subscripts), kmoles;
p - pressure (with scripts) (p_A - ambient pressure above the steel melt), atm;
r_C - chemical reaction rate for nitrogen de-sorption (also r_{C0}), (k)moles $s^{-1}\ m^{-2}\ atm^{-1}$;
r_G - gas phase mass transfer coefficient (nitrogen), kmoles $m^{-2}\ s^{-1}\ atm^{-1}$;
s - trajectory space for the jet (carrier gas + DRI particles), m;

t - time, s;
t_e - "contact" time (duration for the bubble to rise with U_B within as space equaling d_B), m;
x - horizontal coordinate (jet propagation), m;
y - vertical coordinate (bubble rising or jet propagation), m;
% G - gas concentration in the bubble, vol. %;

a - jet (carrier gas + DRI particles) angle (also, a_0 at t = 0), degrees;
a_1 - degree of dissociation of nitrogen molecules into the gas phase, (-);
a_2 - dissociation degree of nitrogen atoms in liquid steel, (-);
b - dimensionless coefficient (= $V_{CO} \times \frac{M_{N_2}(=28)}{224}$), (-);
g - dimensionless coefficient (= $\frac{K_N^2 \times p_{tot}}{h_{CO}^{N_2} \times f_N^2}$), (-);
d - coefficient denoting the system resistance to nitrogen removal, Nm^3 $tonne^{-1}$;
e - parameter correcting the equilibrium nitrogen as result of the chemical reaction, wt. %;
$h_{CO}^{N_2}$ - efficiency of carrier gas, (-);
h_N - efficiency of nitrogen removal, (-);
q - jet (carrier gas + DRI particles) fraction, (-);
n - purging ratio for the carrier gas (defined as in [33]) (with subscripts), (-);
r - liquid steel density, kg m^{-3};
$r_{(\,)}$ - jet (carrier gas + DRI particles) density parameters (with subscripts as in [31]), units;
s - surface tension in the liquid iron, [26], N m^{-1};
Δ - symbol for parameter difference;
$(1-\Theta)$ - fraction of area coverage for nitrogen de-sorption, (-).

REFERENCES:

1. L. B. McFeaters *et al*. – "Solubility of Nitrogen in Liquid Steel in Plasma Induction Reactor", Ironmaking and Steelmaking, UK, no. 4, 1993, pp. 298 - 306.
2. J. Thomas, *et al*. – "Nitrogen Control During EAF Steelmaking", Iron & Steelmaker, Part I – X, vol. 4 (1993) – 1 (1994), pp. 15 – 16, 37 – 38, 41 – 42, 50 – 52, 50 – 52, 61 – 62, 68.
3. G. Brooks, and F. Huo – "High Temperature Behavior of Iron Carbide", 1999 Electric Furnace Conference, pp. 731 - 740.
4. A. Galvez, *et al*. - "Preheating of Hot Briquetted Iron", 1999 EAF Steelmaking Conference Proceedings, Iron and Steel Society, Warrendale, PA, USA, pp. 741 – 749.
5. D. A. Goldstein, *et al*. - "The Behavior of DRI in Slag-Metal Systems and Its Effects on the Nitrogen Content of Steel", Iron and Steelmaker, February 1999, pp. 49 - 61.
6. K. Walden – "Pneumatic Injection of DRI Fines at Hamburgher Stahlwerke", 22nd McMaster University Iron and Steelmaking Symposium", edited by G. A. Irons, 1994, pp. 28 – 38.
7. J. Thomas, *et. al*. – "Nitrogen Control During Electric Furnace Steelmaking", Proceedings of the 50th Electric Furnace Conf., ISS-AIME, 1992: See also EPRI Report TR – 101600, 1992.
8. G. H. Geiger – "Injection In The Electric Furnace: Transformation From An Energy Source To A Chemical Reactor", Keynote Lecture at 22nd McMaster Symposium on Enhancement of EAF Performance by Injection Technology, May 24 – 26, 1994, McMaster University, Hamilton, Ontario, Canada, pp. 1 – 27.
9. G. H. Geiger – "The Use of Iron Carbide in the Electric Arc Furnace", SEAISI Quarterly, July 1994, pp. 57 – 62.
10. G. H. Geiger, and F. A. Stephens – "Steelmaking with Iron Carbide", 1993 Ironmaking Conference Proceedings, ISS-AIME, 1993, Warrendale, PA, pp. 333.
11. R. Garraway – "Nucor's Startup of the World's First Commercial Iron Carbide Plant", Proceedings of the ISS 55th Ironmaking Conference", Iron and Steel Society, Warrendale, PA, USA, 1996.
12. Y. F. Zhao, and G. A. Irons – "Calcium carbide powder injection into hot metal" – Part 2, Ironmaking and Steelmaking, vol. 21 (1994), pp. 309 - 317.
13. D. A. Goldstein, and R. J. Fruehan – "Mathematical Model for Nitrogen Control in OSM", 1998 Steelmaking Conference Proceedings", Toronto, Canada, pp. 259 – 281.
14. D. A. Goldstein – "Nitrogen Reactions In The EAF And OSM", Ph. D. Thesis, Carnegie Mellon University, May 1996, Pittsburgh, PA, USA, pp. 45 – 60, 82 – 85, 159.
15. F. Huo – "The Use of Iron Carbide for the Removal of Nitrogen from Molten Steel", M. Sc. Thesis, University of Wollongong, Australia, 1997, pp. 61 – 131.
16. A. Galvez – "Preheating of Hot Briquetted Iron for Feeding to Electric Arc Furnace Steelmaking", M. Sc. Thesis, University of Wollongong, Australia, 1999, pp. 1 - 261.
17. R. J. Fruehan – "Lectures on Advanced EAF Steelmaking", BHP Research, Port Kembla, Australia, 1995.
18. G. H. Geiger, "Process Engineering Involved in the Use of Direct Reduced Iron" – Chapter XII, DRI – Technology and Economics of Production and Use, pp. 149 - 159.

19. W. Geller – "Zur Theorie der Entgassung flüssiger Metalbäder durch Spülgas", Zeitschrift für Metallkunde, vol. 11, 1943, pp. 213 - 217.
20. P. Vallet, – "Theory of Degassing of the Open-Hearth Bath During Carbon Boil", Iron and Steel, Vol. 28, 463, 1955, pp. 109 - 112.
21. I. V. Yavoiskii – "Steelmaking", Moskow, USSR, 1983.
22. M. S. Lee, *et al.* – "Iron Carbide as a Reagent for Enhanced Nitrogen Desorption in Steel Melts", Iron & Steelmaker, vol. 9 (2003), pp. 55 - 60.
23. G. A. Irons – "Heat Transfer and Lance Clogging During Submerged Powder Injection", Metallurgical Transactions B", vol. 18B, March 1987, pp. 105 – 117.
24. G. A. Irons – "Role of Mixing in Powder Injection Desulphurization Process", Ironmaking and Steelmaking, Vol. 16, no. 1, UK, pp. 28 – 36.
25. E. T. Turkdogan – "Physical Chemistry of High Temperature Technology", Academic Press, NY, USA, 1980.
26. B. Deo, and R. Boom - "Fundamentals of Steelmaking Technologies", Prentice Hall International, New York, 1993.
27. G. R. Belton - "How Fast Can We Go? – The Status of our Knowledge of the Rates of Gas – Liquid Metal Reactions", Metallurgical Transactions, vol. 7B (1993), pp. 241 - 251.
28. M. Byrne, and G. R. Belton – "Studies of the Interfacial Kinetics of the Reaction of Nitrogen with Liquid Iron by the ^{15}N – ^{14}N Isotope Exchange Reaction", Metallurgical Transactions, Vol. 27 (1987), pp. 633 - 637.
29. M. Takahashi, *et al*. – "Rate Controlling Mechanism of Nitrogen Desorption by Ar Injection into Molten Iron", Transaction ISIJ, Vol. 27 (1987), pp. 626 - 632.
30. M. Takahashi, *et al*. – "Enhanced Nitrogen Desorption from Molten Iron by Combined Ar Injection and Blowing", Transaction ISIJ, Vol. 14B (1983), pp. 441 - 449.
31. G. A. Irons, "Fundamental Aspects of Solid Injection", in "Proceedings of the Savard/Lee International Symposium on Bath Smelting", The Minerals and Materials Society, 1992, pp. 493 – 506.
32. Löscher, and Fix – "Applications of a Mathematical Model to Nitrogen Removal in Tank Degassing ", Proceedings of the 1991 Steelmaking Conference Proceedings, Iron and Steel Society, vol. 74 (1991), Warrendale, PA, USA, pp. 669 – 671.
33. D. Papamantellos, *et al*. – "A Mathematical Approach for the Mass Transfer Between Liquid Steel and an Ascending Bubble", Metallurgical Transactions, Vol. 2 (1971), pp. 3135 - 3144.
34. H. Schenck, *et al*. – "Researches on Nitrogen Equilibrium Influence in Liquid Iron as Result of Added Alloying Elements", Archiv für der Eisenhüttenwesen, no. 9, 1959, pp. 533.
35. R. J. Fruehan – "An Introduction to Vacuum Degassing", Iron & Steelmaker, no. 8, 1990, pp. 48 – 49.
36. B. Harkness, *et al*. – "Theoretical and Practical Aspects of Blowhole Formation in Carbon – Steel Ingots", Journal of the Iron and Steel Institute, September 1971, pp. 692 – 713.
37. N. M. Chuiko, – "Theory of Absorption and Elimination of Gases During Smelting and Degassing of Steel", A Special Report – Consultants Bureau, NY, USA, 1965, pp. 11 – 19.
38. J. F. Elliot – "Physical Chemistry of Liquid Steel", Electric Furnace Steelmaking", Iron and Steel Society, 1985, pp. 291 - 319.

39. W. G. Davenport – "Desorption of dissolved gases from liquid metals into rising bubbles – rates of bubble growth", Canadian Metallurgical Quarterly, Vol. (7), No. 3, 1967, pp.127 – 123.
40. J. Kempken, and W. Pluschkell – "Simulationsrechnungen zur Entwicklung der Stickstoffgehalte im LD - Prozeß", Stahl und Eisen, vol. 115 (1995), pp. 67 - 73.
41. K. Harashima, *et al*. - "Rates of Nitrogen and Carbon Removal from Liquid Iron in Low Content Region under Reduced Pressure", ISIJ International, vol. 32 (1992), pp. 111 - 119.
42. V. A. Kudrin – "Steelmaking", Mir Publishers, Moskow, 1985.
43. G. H. Geiger, and D. R. Poirier – "Transport Phenomena in Metallurgy", Addison – Wesley Publishing Co., Reading, Massachussets, USA, 1973., pp. 456 – 458.
44. W. G. Davenport, *et al*. - "Behaviour of Spherical Cap Bubbles in Liquid Metals", Journal of The Iron and Steel Institute, October 1967, pp. 1034 - 1042.